A Quaternary aminostratigraphy for the Pannonian Basin: The competing influences of time, burial depth and temperature in deep-core material

Ellie Nelson [a,*], Zoltán Püspöki [b], Dustin White [a], György Pogácsás [d],
Richard William McIntosh [c], Bálint Szappanos [b], Lucy Wheeler [a], Tamás Fancsik [b],
Kirsty Penkman [a]

[a] Department of Chemistry, University of York, Heslington, York, YO10 5DD, UK
[b] Supervisory Authority for Regulatory Affairs, 1123 Budapest Alkotás u. 50, Hungary
[c] Department of Mineralogy and Geology, Institute of Earth Sciences, Faculty of Natural Sciences and Technology, University of Debrecen, Egyetem Tér 1, 4032, Debrecen, Hungary
[d] Department of Geology, Faculty of Science, Eötvös Lóránd University, 1117 Budapest Pázmány Péter sétány 1/C., Hungary

ARTICLE INFO

ABSTRACT

Long-term terrestrial archives of Quaternary climate change illustrate how global changes affect regional climates, but correlation of terrestrial deposits to global records can be challenging due to a lack of material for radiometric dating. The Pannonian Basin (Hungary) contains large river basins, with near-continuous Quaternary deposits ~600 m in depth. This study tested the IcPD (intra-crystalline protein degradation) approach to amino acid geochronology using bithyniid snail opercula to date deep-core material in geothermally warm regions. Material from seven fully-cored boreholes was collected from four sub-regions: the Körös and Jászság basins, Makó Trough and Békés Basin. IcPD increased with age until approximately 2.3 million years ago, generally supporting stratigraphic correlations previously made between the boreholes. IcPD was consistent between different boreholes within the same sub-region. However due to the steep geothermal gradient in this region, IcPD was systematically different between sub-regions that had different sedimentation rates. Equivalently aged samples buried more deeply had higher IcPD levels, indicating a greater geothermic effect. This provides an insight into how variations in burial temperature can affect protein decomposition within a deeply-buried (>80 m) fossil over geological time, and demonstrates the importance of understanding the geothermal setting for amino acid geochronology. This study shows the utility of IcPD to correlate terrestrial deep-core sediments over the Pleistocene.

1. Introduction

Terrestrial deposits of Quaternary climate change are critical to show how global changes influence regional climates. However, most terrestrial deposits are sporadic and lack continuity (reviewed in Gibbard and Hughes, 2021) and can therefore be challenging to date. Within the European Quaternary record, longer-term archives that represent multiple glacial cycles do occur (e.g. Follieri et al., 1989; Beaulieu and Reille, 1992; Tzedakis et al., 1994, 1999; 2002; Reille et al., 2000; Ortiz et al., 2004a, 2006). Quasi-continuous deposits that cover glacial cycles from the entire Quaternary can be found in tectonically subsiding basins (e.g. Horváth and Cloetingh, 1996; Horváth et al., 2015; Wenau and Alves, 2020). An example of such a record are the Pleistocene fluvial deposits of the Pannonian Basin, Hungary. The Pannonian Basin (Fig. 1) is a large sedimentary basin enclosed by the Carpathian mountain range, currently encompassing all of Hungary, and parts of Slovakia, Ukraine, Romania, Austria, Slovenia and Croatia. Quaternary sediments from the Hungarian part of the Pannonian Basin can be up to ~600 m in depth in the deepest part of the basin (Rónai, 1985; Püspöki et al., 2016). The fluvial deposits lie within an alluvial plain, and contain multiple glacial and interglacial cycles exposed by a set of continuously cored boreholes (Rónai, 1985). The deposition of these archives is controlled by changes in climate: in the Pannonian Basin, glacial conditions are characterised by the deposition of fine-grained sediments due to low transport capacity of the rivers that flowed into it, which are preserved within the subsiding basin. Conversely, interglacials are characterised by coarser

---

* Corresponding author.
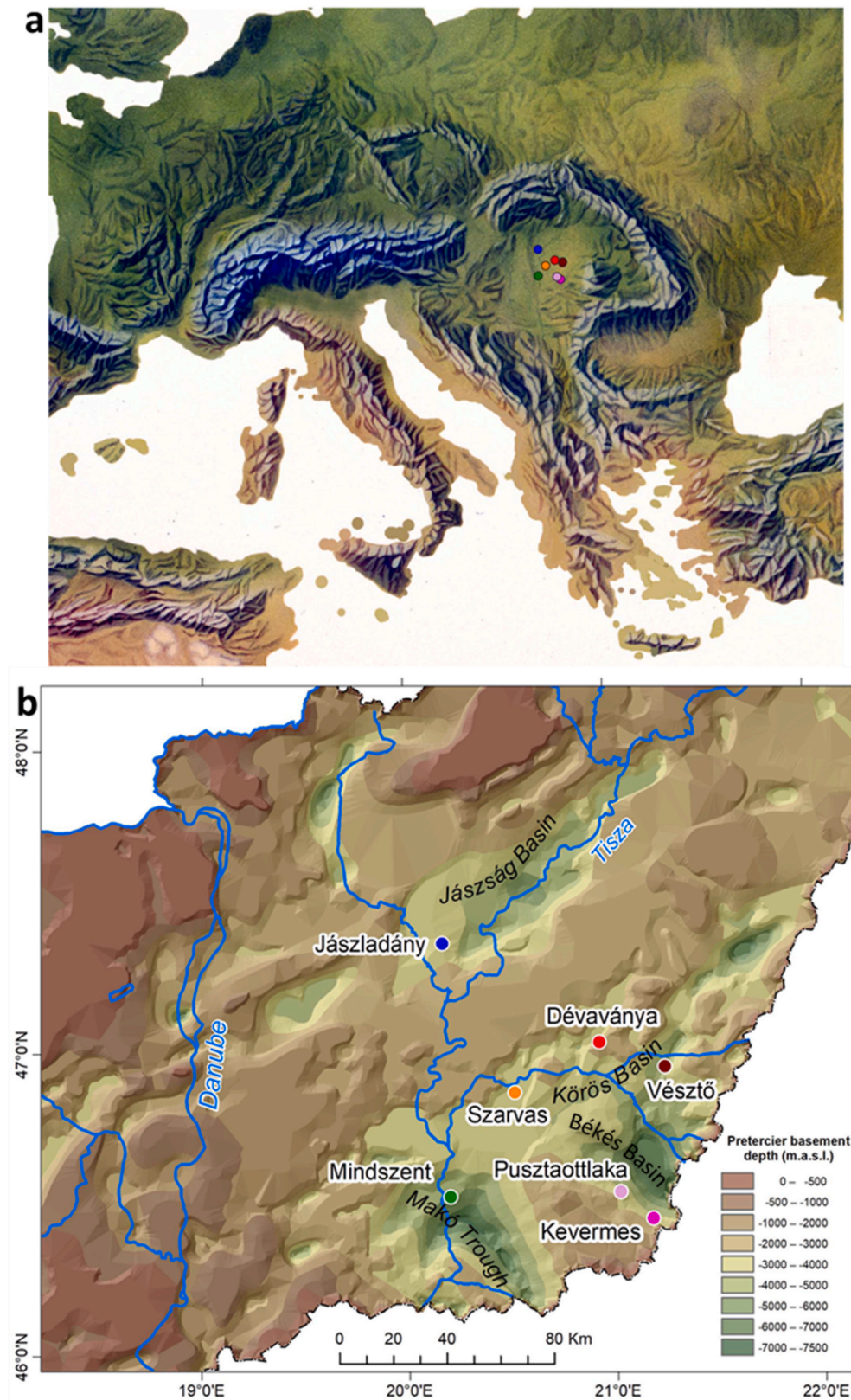 *E-mail address:* ellie.nelson@york.ac.uk (E. Nelson).

Fig. 1. a) Geography of the Pannonian Basin and location of the cores used in this study (colour coding signifies relief of the European topography by Kenneth Townsend); b) Pre-Cenozoic Basement of the Pannonian Basin (Haas et al., 2014) with position of river basins and boreholes analysed (colour coding represents pretercier basement depth/m.a.s.l.).

sediments, as conditions became warmer and wetter (Nádor et al., 2003). Therefore, this area provides an excellent long-term archive to investigate regional changes in climate. However, to do this a robust chronology of these sequences needs to be achieved.

Previous work has attempted to temporally constrain similar cycles, initially by correlating patterns of sedimentation with the classical six Alpine glacial and interglacial stages (Penck and Brückner, 1909; Schaefer, 1953; Häuselmann et al., 2007). Palaeomagnetic investigations (Cooke et al., 1979) confirmed that the Quaternary fluvial deposits of the Körös Basin represent an almost continuous record throughout the Quaternary, with all the relevant palaeomagnetic epochs of the Quaternary determined (e.g. Brunhes, Matayuma with the Jaramillo, Olduvai and Reunion). This was later supported by the observations of sedimentary and magnetic susceptibility investigations which revealed Milankovitch-scale cycles in the fluvial succession (Nádor et al., 2003). In addition, a large set of short lived palaeomagnetic reversals were also identified and confirmed with the Geomagnetic Instability Time Scale (Singer, 2014), corroborating that the Quaternary section of the Körös Basin is complete for all identifiable palaeomagnetic reversals (Püspöki et al., 2021b; Fig. 6). A subsequent re-interpretation of the fluvial magnetic susceptibility as a proxy for early postglacial collapse of mountainous permafrost in the catchment region has enabled correlation of the fluvial cycles in the Körös Basin to the long-term loess sequences of the Chinese Loess Plateau (Ding et al., 2005; Püspöki et al., 2016) and to the MIS record (Lisiecki and Raymo, 2005; Püspöki et al., 2021a). This revised interpretation of the fluvial magnetic susceptibility has also enabled regional-scale correlations of the Quaternary fluvial succession between different sub-basins of the Pannonian Basin, including the Jászság Basin (Püspöki et al., 2020), Makó Trough (Püspöki et al., 2021b), and Békés Basin (Püspöki et al., 2023). The correlation between the Körös Basin and the other sub-basins was supported by accessory biostratigraphic data and verified by multi-proxy spectral investigations.

To ensure a robust chronology is established, independent dating methods are needed to cross-check correlations between the cores and to other long-term climate archives. Aminostratigraphy has been used as a tool to constrain and validate a variety of stratigraphic models using a variety of different biominerals (e.g. Miller and Mangerud, 1985; Hearty and Aharon, 1988; Knudsen and Sejrup, 1988; Goodfriend, 1989; Ortiz et al., 2004b; Wehmiller et al., 2010; West et al., 2019; Preece et al., 2020; Tesakov et al., 2020; Chauhan et al., 2022). Aminostratigraphic dating frameworks are valid within a region that has experienced an equivalent integrated temperature history (Wehmiller and Miller, 2000). Regional aminostratigraphies using the calcitic opercula of bithyniid snails and the intra-crystalline protein decomposition (IcPD) method of amino acid dating (Penkman et al., 2008) have been developed for the British Isles & the Netherlands (Penkman et al., 2013; Preece et al., 2020), the East European Plain (Tesakov et al., 2020), and the Swiss Plateau (Penkman et al., 2024). The intra-crystalline fraction of *Bithynia* (Penkman et al., 2008) and *Parafossarulus* (Tesakov et al., 2020) opercula have been shown to exhibit closed system behaviour for the degradation of the endogenous protein. As such, the IcPD should be solely dependent on time and temperature (Brooks et al., 1990; Penkman et al., 2011, 2013). Bithyniid snail opercula are present within multiple horizons across seven fully cored boreholes from the Pannonian Basin (Krolopp, 1995, 2014), so they provide an opportunity to examine the chronology developed by Püspöki et al. (2013, 2016, 2020, 2021a, 2021b, 2023) by aminostratigraphy.

As the rate of IcPD is dependent on temperature, the depth beneath the surface of the material may affect the temperature it has been exposed to over time. The integrated temperature experienced by material buried close to the surface is influenced significantly by the climate (e.g. Wehmiller, 1982; Wehmiller and Stecher, 2000; Penkman et al., 2011); the rate of protein decomposition increases exponentially with rises in temperature, and therefore will be significantly faster in warm climate episodes, and will slow (or pause completely) in cold

stages (e.g. Bates, 1993; Miller et al., 1999; Penkman et al., 2013). As material is buried deeper beneath the ground, the climate influence weakens and the integrated temperature will be dominated by subsurface factors, such as the geothermal gradient (Fig. 2); the depth of this transition varies across Europe (Pouloupatis et al., 2011; Tinti et al., 2018). These factors will affect how temperature varies with depth, meaning that for some regions, subsurface ground temperatures will remain near constant for 100s of metres below the surface, whereas in other regions temperatures will increase much more steeply with depth.

Previous authors have recognised the potential influence of geothermal heating on protein decomposition in fossilised biominerals located 200–500 m.b.s.l. in deep sea cores (e.g. Bada and Luyendyk, 1971; Bada et al., 1974; Bada and Man, 1977; Blunt et al., 1981; Katz et al., 1983). In these studies, it was noted that samples that were subject to a higher heat flow (geothermal gradient) and sedimentation rate, a greater extent of racemisation/epimerisation was observed (Man et al., 1975; Katz et al., 1983). However, this has not yet been discussed in material gathered for amino acid dating from terrestrial deep cores (e.g. Ortiz et al., 2004b). As the Pannonian Basin is a geothermally hot region (Bodri, 1981; Horváth et al., 2015), the potential influence of geothermal heating on the samples used in this study needs to be considered.

Therefore, this paper presents the first test of the IcPD approach to build an aminostratigraphy from material deeper than 63 m below the surface (Preece et al., 2020). This was achieved by using the D/L values of multiple amino acids to correlate stratigraphic levels between each borehole. First, it was determined whether a closed system has been retained within opercula collected from the Pannonian Basin deep-core sediments recovered from 5 to 463 m below the surface. Next, the viability of this IcPD approach to produce a time signal from deep sediments in each core was examined. Once established, the relationship between the extent of IcPD and the temperature experienced in each core by the opercula samples was assessed. Finally, the aminostratigraphy developed for these cores was compared to other parts of Europe to evaluate the differences between IcPD in deep-core and shallow material.

2. Materials and method

2.1. Geographical and geological setting of the sites

The Great Hungarian Plain is the westernmost unit of the Eurasian Steppe enclosed in the Carpathian Basin, the largest terrestrial basin in Europe. Its annual temperature is 10.5–11.5 °C, with low annual precipitation (500–600 mm per year; 1991–2020; Hungarian Meteorological Service, 2024), meaning the basin possesses a continental climate that is amplified by the orographic effects of the surrounding mountains.

Its recent physical geography is dominated by rivers, their floodplains and by interfluves with windblown sand and loess surfaces; thus its surface is a plain, ranging from 75 to 183 m above sea level. Although the entire Quaternary palaeogeography is considered to be similar (Gábris and Nádor, 2007), the considerable isopach data ranges from 150 to 700 m (Franyó, 1992), indicating that the different parts of the area subsided at different rates during the last 2.5 Ma. The four most important sub-basins are the Körös Basin, Jászság Basin, Békés Basin and Makó Trough (Fig. 1).

The Körös Basin was predominantly filled up by the Palaeo-Tisza and tributaries from the north and north-east, together with the Körös and Sebes-Körös from the east. Occasional and small inputs (around Szarvas) came from the Palaeo-Danube from the north-west and the Palaeo-Maros from the south (Thamó-Bozsó et al., 2002; Thamó-Bozsó and Kovács, 2007). The 450–500 m thick fluvial succession at the Dévaványa, Vésztő and Szarvas sites represent distal sources of continuous fluvial conditions manifested in 5–10 m thick sand bodies representing channel complexes, associated with thick series of sandy silt, silt and clayey silt materials settled on extended floodplains.
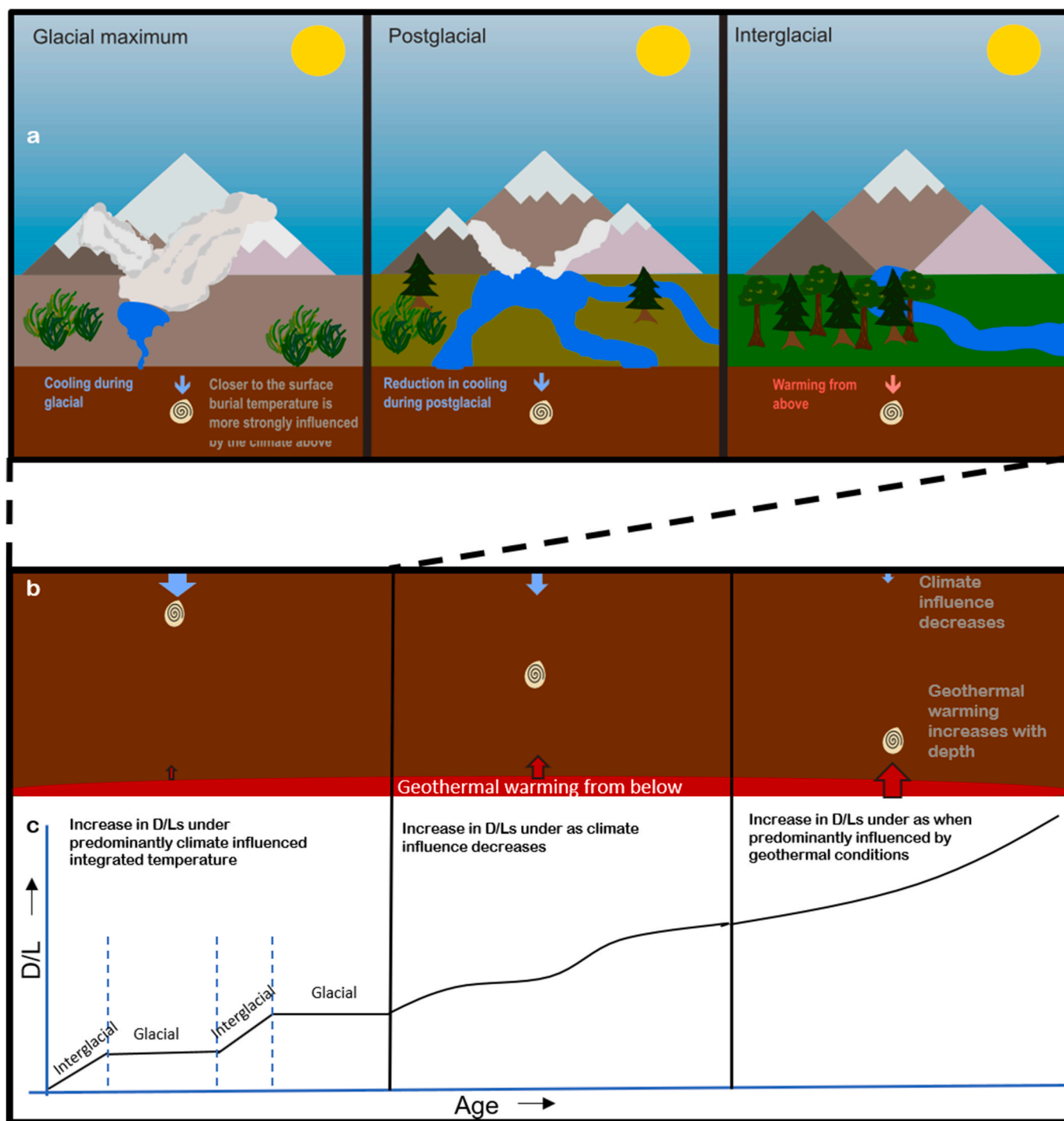
Fig. 2. Schematic demonstrating the influences on temperature experienced by a fossil operculum during burial. a) The temperature experienced by opercula buried close to the surface is more strongly influenced by mean annual temperature, and will experience a cooling or warming effect depending on conditions above. b) Relationship between D/L and time, demonstrating the changing influences on integrated temperature as the opercula moves through sediment column. As the sample is buried deeper underground, the surface temperatures are buffered. With increasing depth, the temperature experienced will be more strongly influenced by sub-surface factors such as geothermal gradient. The extent of IcPD experienced by a sample will therefore be due to the combined effects, from its initial shallow deposition to continued burial further below the surface until excavation.

The central part of the Jászság Basin at Jászladány was not reached by the Tisza or Danube but by small watercourses draining the North Hungarian Mountain Range and NW Carpathians. Thus, the 370 m thick Quaternary fluvial succession is characterized here by 2–5 m thick sand bodies representing channel sand complexes of the small rivers, embedded into thick series of sandy and clayey silt successions of overbank settings (Rónai, 1985; Püspöki et al., 2020).

The Békés Basin is at the south-east part of the Great Hungarian Plain and was filled during the Quaternary by the Maros fluvial fan. It is the best-preserved fluvial fan succession of the Pannonian Basin (Püspöki et al., 2023 Fig. 1). In the Kevermes and Pusztaottlaka boreholes it is represented by a 430–500 m thick upward coarsening succession of channel sands and overbank fines, with upwards increasing number and thickness of sand bodies.
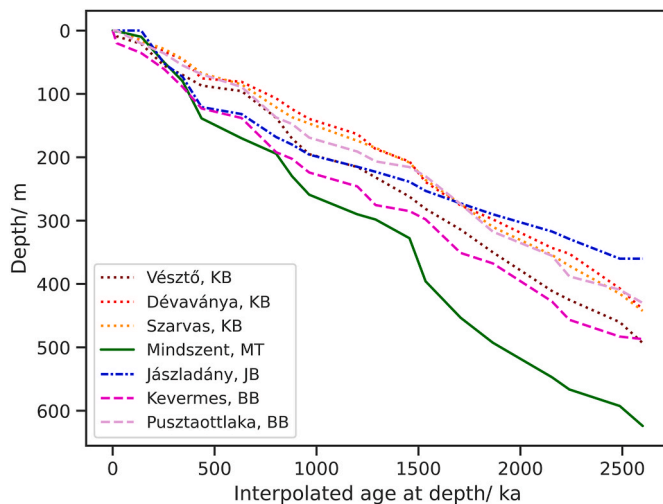
Fig. 3. Interpolated age for each MP vs. depth (described in Püspöki et al. (2021b, 2023)). This demonstrates how the rate of sedimentation varies between the cores. Dotted lines represent cores from the Körös Basin (KB), the continuous line represents the core from the Makó Trough (MT), dash/dotted line represents the core from the Jászság Basin (JB), and dashed lines represent the cores from the Békés Basin (BB).

The Makó Trough is the main centre of the Pleistocene drainage network of the Pannonian Basin reached by the Palaeo-Danube, Palaeo-Tisza and their tributaries. Although the margins to the north and west of the Makó Trough were affected by Quaternary structural events, its central part at Mindszent seems to be a complete sequence (Püspöki et al., 2021b). Due to the frequent occurrence of different but large rivers, the 630 m thick Quaternary fluvial succession is mostly characterised by 10 m thick sand bodies embedded into successions of overbank fines.

The Quaternary succession of the cores studied (Fig. 1) had previously been divided into magnetically identified sedimentary cycles (MS cycles; Table 1; Püspöki et al., 2013, 2016, 2020, 2021a, 2021b, 2023). These cycles are capped by their most significant diagnostic magnetic susceptibility peak (MP; Table 1), and sometimes contain characteristic secondary peaks. The tops of MPs are termed 'susceptibility termination surfaces' (STS); these regional decreases in MS values are interpreted as periods of increased weathering due to warming during interglacials, resulting in a reduction of magnetic minerals from the sedimentary load (Püspöki et al., 2016).

MPs identified in the Körös Basin (Dévaványa, Vésztő) have been correlated with the cold stages of the MIS records (Lisiecki and Raymo, 2005). MS cycles VI-X are correlated with the significant Early Pleistocene glaciations, and MS cycles I-V with the substantial Middle and Late Pleistocene European glaciation events (Table 1, data derived from Püspöki et al., 2021b Fig. 6).

Palaeomagnetic boundaries have not been established across the sub-basins of the Makó Trough and Jászság Basin, so biostratigraphy provided an independent tool to support cross-correlation. The molluscan fauna of the Pannonian Early and Middle Pleistocene is characterised by extinct or emigrant forms (Krolopp, 1995, 2014). The last appearance datum of *Viviparus boeckhi* (LAD Vb, ~550 ka) occurs within the MS cycle III, while the first appearance datum (FAD Vb, ~1.75 Ma) coincides with the magnetic susceptibility cycle VIII (Püspöki et al., 2016). The cross-basin correlations based on the MS cycles were tested by a time series analysis of additional re-scaled variables (e.g. log-derived grain size proxies and computer aided colour measurements). Since these proxies were not used to determine the age-depth relationship, the Multi-Taper method spectra of these variables are significant, as they enable the detection of Milankovitch frequencies in these records, suggesting that the age model of the section is accurate (Püspöki et al.,

Table 1

Description of the magnetic susceptibility (MS) cycles and magnetic susceptibility peaks (MP) found across the three sub-basins (Körös, Jászság, Makó Trough and Békés Basin) defined by Püspöki et al. (2016, 2020, 2021a; 2021b). MS cycles are capped by 'susceptibility termination surfaces' followed by the most significant MS peak within the cycle (MP). MS cycles are denoted by Roman numerals and MPs by the corresponding Arabic number. Significant secondary peaks within a MS cycle are indicated by Arabic numbers and a letter. MPs have been correlated with MIS cold stages, with age assignment made on the basis of the stacked $\delta^{18}O$ chronology (Lisiecki and Raymo, 2005). The first (FAD) and last (LAD) appearance of the freshwater gastropod *Viviparus boeckhi* has been used to constrain the age correlations of MS III and VIII (Krolopp, 1970). Depths of the master peak for each core can be found in the supplementary information.

Magnetic Susceptibility Cycle	Master Peak	Correlated MIS	Age assignment/ka
0	0	2	20
I	1	6	140
II	2	8	252
	2a	10	343
III (LAD: 550 ka)	3	12	436
	3a	16	632
IV	4	20	802
	4a	22	880
V	5	26	964
VI	6	34–36	1200
	6a	40	1290
	6d	48	1456
VII	7	52	1535
VIII (FAD: 1.8 Ma)	8	60	1707
	8a	68	1865
IX	9	82	2155
	9a	86	2240
X	10	98	2488
	10a	104	2600

2020, 2021a).

The age of each horizon containing opercula that was sampled for this study was estimated via linear interpolation (Püspöki et al., 2021a&b). In the present study, the uncertainty in those ages was estimated using a Monte Carlo approach (Kalos and Whitlock, 2009), carried out using the following steps. Firstly, a nominal uncertainty of 5% (chosen as a rough estimation of the error) was assumed for the assigned ages outlined in Table 1, with a minimum uncertainty of 1 ka. For each assigned age, a normally distributed synthetic dataset of age values was generated (n = 10,000; normal distribution has been assumed but may not be an accurate representation of the error) with the standard deviation equal to the assumed uncertainty. The synthetic dataset was then used to derive a distribution of interpolated ages for the mid-point of the depth range for each of the sample horizons. The standard deviation of the interpolation was then used to estimate the respective uncertainty for the age of each horizon. The Monte Carlo method was performed using the "numpy" package from Google Colab with Python (3.10).

2.2. Materials

Three species of bithyniid snails were identified throughout the seven cores, but were not present in all MS cycles in each core. The opercula of bithyniid snails are mineralised in the form of calcite, the most stable pseudomorph of calcium carbonate (de Leeuw and Parker, 1998), and shown to provide a closed system for intra-crystalline amino acids as old as the Eocene (Penkman et al., 2013). The species analysed here were *Bithynia leachii* and *Bithynia tentaculata* (Table 2). Samples were selected in order to encompass the largest temporal range across the Quaternary; this included, where possible, from the top and bottom of each magnetic susceptibility cycle. *B. leachii* opercula were initially selected for this analysis, as they were more consistently present in the upper parts of each core. *B. tentaculata* opercula were selected where additional material was required to improve understanding of trends

Table 2

Bithyniid snail opercula analysed in this study together with the depth below the surface that the samples were recovered from, the lithology, texture, and palaeomagnetic orientation of the surrounding sediments, and age interpretation defined by Püspöki et al. (2013, 2016, 2020, 2021a, 2021b, 2023). The 'NEaar no.' is the identification number for each fossil sample analysed in the laboratory.

Site/Core	Depth below surface	Palaeomagnetic Orientation (Cooke et al., 1979)	Magnetic Susceptibility Cycle (Püspöki et al., 2016, 2020, 2021a, 2021b)	Master peak directly above sample depth (Püspöki et al., 2021b)	Interpolated Ages in ka (Püspöki et al., 2021b)	Number of opercula analysed	Species	Lithology	Texture	NEaar No.
Dévaványa (Körös Basin)	5.38–5.54 m	Normal	Before I	Above 1	49	3	*B. leachii*	clayey silt	massive	14329–14331
	29.41–30.37 m	Normal	I (near I/II boundary)	1	229	3	*B. leachii*	sandy silt	laminated	14332–14334
	36.66–37.13 m	Normal	II	2	278	2	*B. leachii*	sandy silt	laminated	14335–14336
	75.23–75.37 m	Normal	III	2a	436	3	*B. leachii*	silty sand	massive	14337–14339
	129.60–131.05 m	Reversed	IV	4a	914	2	*B. leachii*	clayey silt	massive	14340–14341
	194.90–195.28 m	Reversed	VI	6a	1358	2	*B. leachii*	clayey silt	massive	14342–14343
Vésztő (Körös Basin)	25.20–25.89 m	Normal	I	1	155	3	*B. leachii*	sandy silt	massive	14344–14346
	81.26–81.68 m	Normal	III (near II/III boundary)	2	404	3	*B. tentaculata*	clayey silt	massive	15871–15873
	82.00–83.16 m	Normal	III	2	411	3	*B. tentaculata*	sandy silt	massive	15874–15876
	94.25–97.00 m	Normal	III	3a	633	5	*B. leachii*	sand	laminated	14347-14349, 15006-15007
	98.10–98.85 m	Normal	III	3a	644	3	*B. tentaculata*	silty sand	non documented	15877–15879
	137.43–138.00 m	Normal	IV	4	802	3	*B. leachii*	silty sand	laminated	14350–14352
	159.98–160.48 m	Reversed	IV	4	856	5	*B. leachii*	sandy silt	laminated	14353-14355, 15004-15005
	231.03–231.78 m	Reversed	VI	6	1289	4	*B. leachii*	sandy silt	laminated	14655–14658
	431.16–432.00 m	Reversed	IX	9	2294	2	*B. leachii*	clayey silt	laminated	14356–14357
Szarvas (Körös Basin)	10.65–11.00 m	N/A	I	0	92	3	*B. leachii*	silty sand	non-documented	15122–15124
	19.46–19.68 m	N/A	I	1	168	3	*B. leachii*	sandy silt	massive	15125–15127
	52.62–54.00 m	N/A	II	2a	378	2	*B. leachii*	clayey silt	massive	15128–15130
	84.40–84.82 m	N/A	III	3	629	2	*B. leachii*	sandy silt	laminated	15131–15132
	97.39–97.56 m	N/A	III	3a	691	3	*B. leachii*	silty sand	non-documented	15133–15134
	117.90–118.69 m	N/A	III	3a	789	3	*B. leachii*	clayey silt	massive	15135–15137
	125.13–126.06 m	N/A	IV	4	824	3	*B. leachii*	clayey silt	massive	15138–15140
	140.10–140.61 m	N/A	IV	4a	910	3	*B. leachii*	clayey silt	massive	15141–15143
	270.85–271.51 m	N/A	VII	7	1696	2	*B. leachii*	sandy silt	massive	15144–15145
	319.84–320.62 m	N/A	VIII	8	1966	3	*B. leachii*	clayey silt	laminated	15146–15148
	393.75–393.88 m	N/A	IX	9a	2366	2	*B. leachii*	silty sand	ripple laminated	15149–15150
	442.34–442.49 m	N/A	X	10	2600	2	*B. leachii*	silty sand	massive	15151–15152
Mindszent (Makó Trough)	17.56–18.64 m	N/A	I	1	159	3	*B. leachii*	silty clay	massive	15603–15605

Table 2 (*continued*)

Site/Core	Depth below surface	Palaeomagnetic Orientation (Cooke et al., 1979)	Magnetic Susceptibility Cycle (Püspöki et al., 2016, 2020, 2021a, 2021b)	Master peak directly above sample depth (Püspöki et al., 2021b)	Interpolated Ages in ka (Püspöki et al., 2021b)	Number of opercula analysed	Species	Lithology	Texture	NEaar No.
	109.63–109.68 m	N/A	II	1	369	3	*B. leachii*	sandy silt	massive	15606–15608
	136.22–136.55 m	N/A	III	1	431	3	*B. leachii*	sandy silt	massive	15609–15611
	177.60–180.00 m	N/A	III	3	700	3	*B. leachii*	silty sand	non-documented	15612–15614
	206.53–206.61 m	N/A	IV	4	832	3	*B. leachii*	silty sand	ripple laminated	15615–15617
	275.35–276.10 m	N/A	V	5	1102	3	*B. leachii*	silty clay	massive	15618–15620
	287.69–288.26 m	N/A	V	5	1204	3	*B. leachii*	sandy silt	laminated	15621–15623
	329.80–330.28 m	N/A	VI	6d	1459	3	*B. leachii*	silty clay	massive	15624–15626
	422.61–422.99 m	N/A	VII	7	1616	1	*B. leachii*	silt	massive	15627
	431.26–431.54 m	N/A	VII	7	1641	2	*B. leachii*	clayey silt	massive	15628–15629
	468.14–469.39 m	N/A	VIII	8	1769	3	*B. leachii*	silt	massive	15630–15632
Jászladány (Jászság Basin)	43.47–44.00 m	N/A	I	0	212	3	*B. leachii*	silty clay	massive	15771–15773
	55.90–56.64 m	N/A	II	2	273	3	*B. leachii*	silty clay	massive	15774–15776
	102.55–102.80 m	N/A	II	2a	401	3	*B. leachii*	silty clay	massive	16511–16514
	114.53–114.71 m	N/A	II	2a	424	5	*B. leachii*	silty clay	massive	15777–15779
	118.70–118.86 m	N/A	III	2	432	5	*B. leachii*	silty clay	massive	15780–15782
	125.52–125.77 m	N/A	III	3	523	3	*B. leachii*	sandy silt	massive	16515–16517
	149.15–149.19 m	N/A	III	3a	676	5	*B. leachii*	sandy silt	massive	15783–15785
	149.15–149.19 m	N/A	III	3a	713	4	*B. tentaculata*	sandy silt	massive	16521–16524
	165.66–165.87 m	N/A	IV	4	791	2	*B. tentaculata*	sandy silt	massive	16525–16526
	208.85–209.03 m	N/A	V	5	1121	4	*B. tentaculata*	silty clay	massive	16529–16532
Kevermes (Békés Basin)	74.50–75.00 m	N/A	II	2	297	5	*B. leachii*	silty sand	laminated	16931–16934
	116.00–116.20 m	N/A	II	2	417	4	*B. leachii*	silty sand	massive	16929-16930, 16935
	133.00–133.50 m	N/A	III	2a	570	3	*B. leachii*	silty clay	massive	16927–16928
	174.00–174.50 m	N/A	III	3	746	4	*B. leachii*	sand	non-documented	16923–16926
	310.00–311.50 m	N/A	VII	3a	1576	3	*B. leachii*	silty sand	massive	16922–16923
Pusztaottlaka (Békés Basin)	61.50–62.50 m	N/A	II	2	256	4	*B. leachii*	silty clay	massive	16919–16921
	79.00–79.50 m	N/A	III	3	536	3	*B. leachii*	sand	non-documented	16916–16918
	114.50–115.00 m	N/A	III	3a	723	5	*B. leachii*	silty clay	massive	16911–16915

Table 2 (*continued*)

Site/Core	Depth below surface	Palaeomagnetic Orientation (Cooke et al., 1979)	Magnetic Susceptibility Cycle (Püspöki et al., 2016, 2020, 2021a, 2021b)	Master peak directly above sample depth (Püspöki et al., 2021b)	Interpolated Ages in ka (Püspöki et al., 2021b)	Number of opercula analysed	Species	Lithology	Texture	NEaar No.
	338.00–338.30 m	N/A	VIII	8a	2023	4	*B. leachii*	silty sand	laminated	16907–16910
	432.80–438.20 m	N/A	Pliocene	10a	≥2600[a]	4	*B.* sp.	silty sand	ripple laminated	16903–16906

[a] An age of 2600 ka is used for this horizon/sample, but this is a minimum age as samples have been attributed to the Pliocene and are beyond the scope of the age model.

observed in the data. The extent of protein decomposition varies between different taxa of biominerals, but the difference in overall IcPD between the different species used here has so far been found to be minimal (Penkman et al., 2007, 2013; Tesakov et al., 2020), so congeneric species will be compared directly in this study.

2.3. Analysis

All samples were prepared using the procedures outlined in Penkman et al. (2008), a method that isolates the intra-crystalline protein fraction by oxidation. Between one to five individual opercula were analysed from each horizon (see Table 2). In brief, following oxidation by sodium hypochlorite for 48 h (NaOCl) of the powdered samples (crushed to ≲0.425 mm; Penkman et al., 2008), two fractions were taken from each operculum. The first fraction was demineralised using 2 M hydrochloric acid (HCl) in order to analyse the naturally occurring free amino acids (FAA) within the sample. The second fraction was used to analyse the total hydrolysable amino acid content (THAA), by hydrolysing the peptide bonds at 110 °C for 24 h using 7 M HCl. This step also induced demineralisation of the biomineral. Analytical duplicates were performed for both the FAA and THAA fractions from each individual operculum (unless specified otherwise in Appendix B) alongside standards and blanks using a modified version of the reverse-phase high-performance liquid chromatography (RP-HPLC) method described by Kaufman and Manley (1998). Unless specified otherwise the mean D/L value of all opercula samples from the same horizon are presented ±1 σ. This method separates the L- and D-isomers of 12 commonly occurring amino acids: aspartic acid/asparagine (Asx), glutamic acid/glutamine (Glx), serine (Ser), arginine (Arg), alanine (Ala), tyrosine (Tyr), valine (Val), phenylalanine (Phe), isoleucine (Ile) and leucine (Leu). The extent of racemisation is quantified by calculating the ratio of D to L, which is described by the D/L value. Asparagine and glutamine irreversibly degrade to aspartic acid and glutamic acid, respectively, due to deamination during the hydrolysis step (Hill, 1965) and are therefore reported as Asx and Glx.

In a closed system, the FAA and THAA D/L values should be highly correlated for each amino acid, and lack of correlation helps to identify compromised samples (Preece and Penkman, 2005). The D/L value will increase over time, at different rates for each amino acid, which allows for better temporal resolution over different time scales (Goodfriend, 1991). The best chromatographically resolved enantiomeric pairs for bithyniid opercula are Asx, Glx, Ser, Ala and Val (Penkman et al., 2013; Powell et al., 2013). Ser is geochemically unstable compared to other amino acids, decomposing to alanine in addition to other organic molecules (Bada et al., 1978). As such, it is not a useful geochronometer for the Pleistocene, but is useful as a marker for contamination (e.g. Kosnik and Kaufman, 2008). Asx, Glx, Ala and Val cover a wide temporal range (Penkman et al., 2011, 2013) so were therefore used to provide an estimate of the overall IcPD in this study.

Data analysis was performed using Google Colab with Python (3.10). The D/L values for both FAA and THAA samples are reported as the mean D/L value for a given horizon, and incorporates all the specimens analysed for that horizon. The uncertainty was presented as 1 σ for each horizon. For clarity, the samples from each of the seven boreholes have been colour coded as follows throughout the paper: Vésztő = maroon, Dévaványa: red, Szarvas = orange, Mindszent = green, Jászladány = blue, Pusztaottlaka = pale purple and Kevermes = pink.

3. Results & discussion

3.1. Testing for closed system behaviour

Following cessation of tissue turnover within an organism, proteins degrade via three key pathways, which co-occur. The first is the hydrolysis of peptide bonds to yield short peptide chains and ultimately free amino acids, increasing %FAA. Secondly, amino acids decompose to
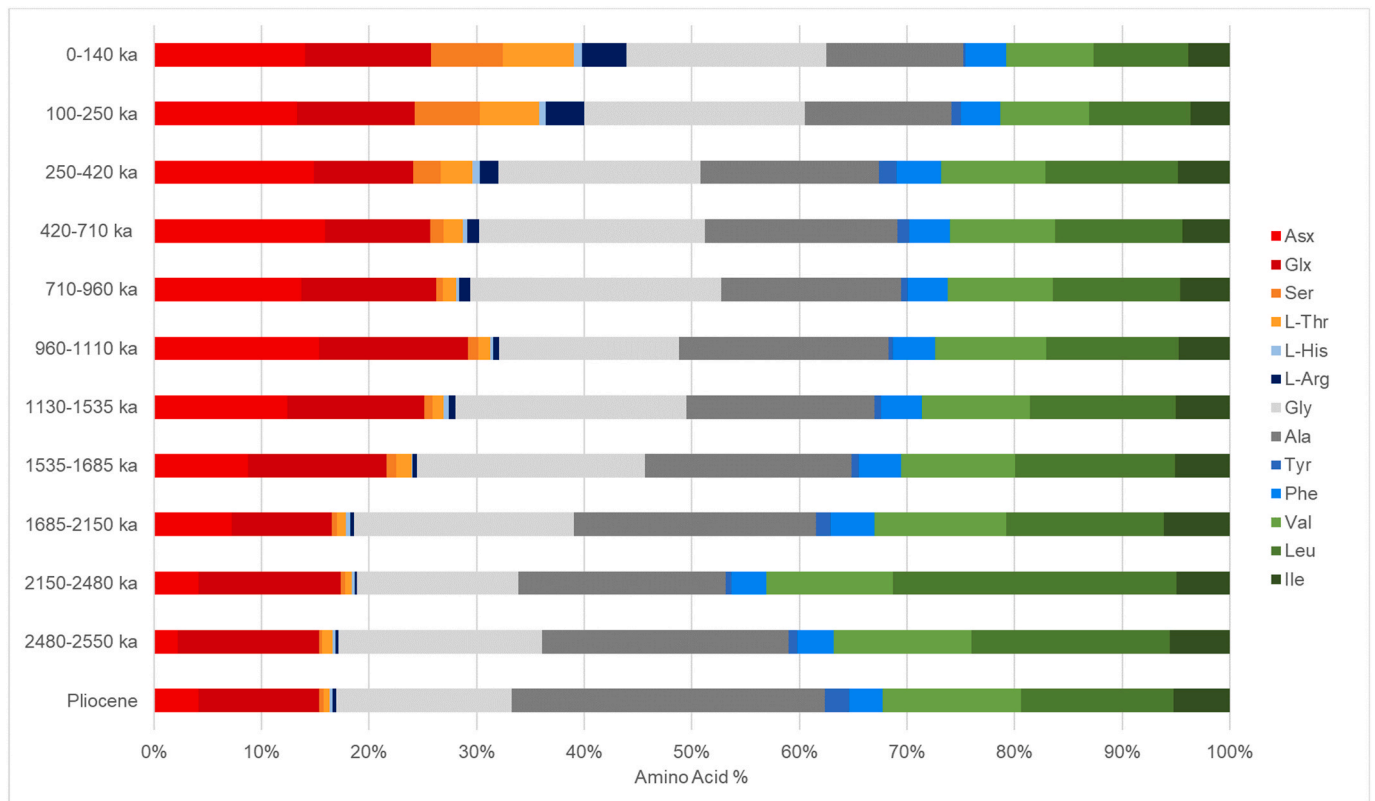
Fig. 4. Mean intra-crystalline amino acid compositions for opercula from all seven cores of each MS cycle THAA fractions. Younger samples possess higher proportions of the polar amino acids (red, orange and blue); samples of greater antiquity possess higher proportions of non-polar amino acids (green and grey).

other more stable amino acids (e.g. the proportion of alanine and glycine in older material is contributed to by the decomposition of other amino acids; Bada et al., 1978; Kossiakoff, 1988; Sato et al., 2004; Penkman et al., 2008), and ultimately smaller organic molecules such as ammonia and carbon dioxide (Boyer et al., 1959; Bada et al., 1978). Therefore, the composition of amino acids within a sample provides an indication of age. Thirdly, amino acids spontaneously racemise between the L and D forms. During biomineralisation only the L amino acid is incorporated into the protein structure, but when tissue turnover ceases, the proportion of D-amino acids will increase due to racemisation, eventually resulting in a racemic equilibrium. The D/L values provide the most reliable measure of decomposition, but others can provide corroborative evidence (Miller and Hare, 1975).

%FAA is more variable than other parameters (Penkman et al., 2013; due to the inherent errors in mass and volume (Powell et al., 2013) as well as the decomposition of FAA during the hydrolysis procedure to isolate the THAA), but in general %FAA increased with age. For example, the %FAA of the youngest samples (Dévaványa 5.38–5.54 m, ~50 ka; Püspöki et al., 2021a) was ~42%, compared to ~ 95% in the oldest samples (432.8–438.2 m, Pliocene; Püspöki et al., 2023 indicating greater protein decomposition within these samples).

In this dataset, as expected the shallower/younger samples have greater proportions of Asx and Ser, whereas in deeper/older samples these contribute less to the overall amino acid composition (Fig. 4). Conversely, the proportion of more stable amino acids such as Ala and Val increase over time (Fig. 4). The change in amino acid composition supports the conclusion that the proteins in the opercula tested here become more degraded with age and depth.

If a closed system has been retained within the samples analysed, the D/L value of both the THAA and FAA fractions should be highly correlated in all amino acids. For the vast majority of samples, all their amino acids analysed show good correlation between the THAA and FAA fractions (Fig. 5; 96% of samples, Fig. 5), with a few interesting

exceptions. These were extreme visual outliers from the expected trend, highlighted in Fig. 5. A number of samples did not yield results for one of the two fractions (2% of FAA and 3% of THAA) due to small sample size, resulting in the amino acids extracted being below the method's detection limits. All outliers where the closed system within the sample has been lost, or the composition or relative rate of racemisation does not conform to that expected (e.g. Preece and Penkman, 2005) are reported in the SI. These have been excluded from the calculation of the means of the data from each horizon in the following sections of this study. Where samples have provided data for only one of the two fractions, this has been included in the mean calculation for that fraction.

3.2. Extent of IcPD with depth

The D/L values for all amino acids rise with increasing depth; Ala reaches equilibrium for the deepest samples (Fig. 6b), while Glx & Val approach equilibrium (Fig. 6c and d). Asx racemises rapidly but also starts to degrade in the oldest samples (Fig. 4), resulting in an apparent decrease in Asx D/L (Fig. 6a) in the deepest horizons of the Putztaottlaka, Mindszent & Vésztő cores (also observed in Penkman et al., 2013). All samples with lower than expected Asx D/L values came from opercula located greater than 330 m in depth and were attributed to MS cycles 7 to 10 for Vésztő and Mindszent. The Pusztaottlaka operculum came from Pliocene age sediments with a minimum age of 2.6 Ma. As shown in Fig. 4, the % concentration and quantity of Asx significantly reduces in the oldest material. This is likely due to the relative instability of this amino acid compared to the other amino acids presented (e.g. Brooks et al., 1990; Bada et al., 1999). Penkman et al. (2013) observed a similar decrease in Asx D/L values in Eocene aged opercula from the Isle of Wight. Loss of both L- and D-isomers of Asx due to chemical breakdown means that the Asx D/L values within the oldest samples are no longer directly indicative of the age of the sample, but this can be recognised by the low concentrations and % composition.
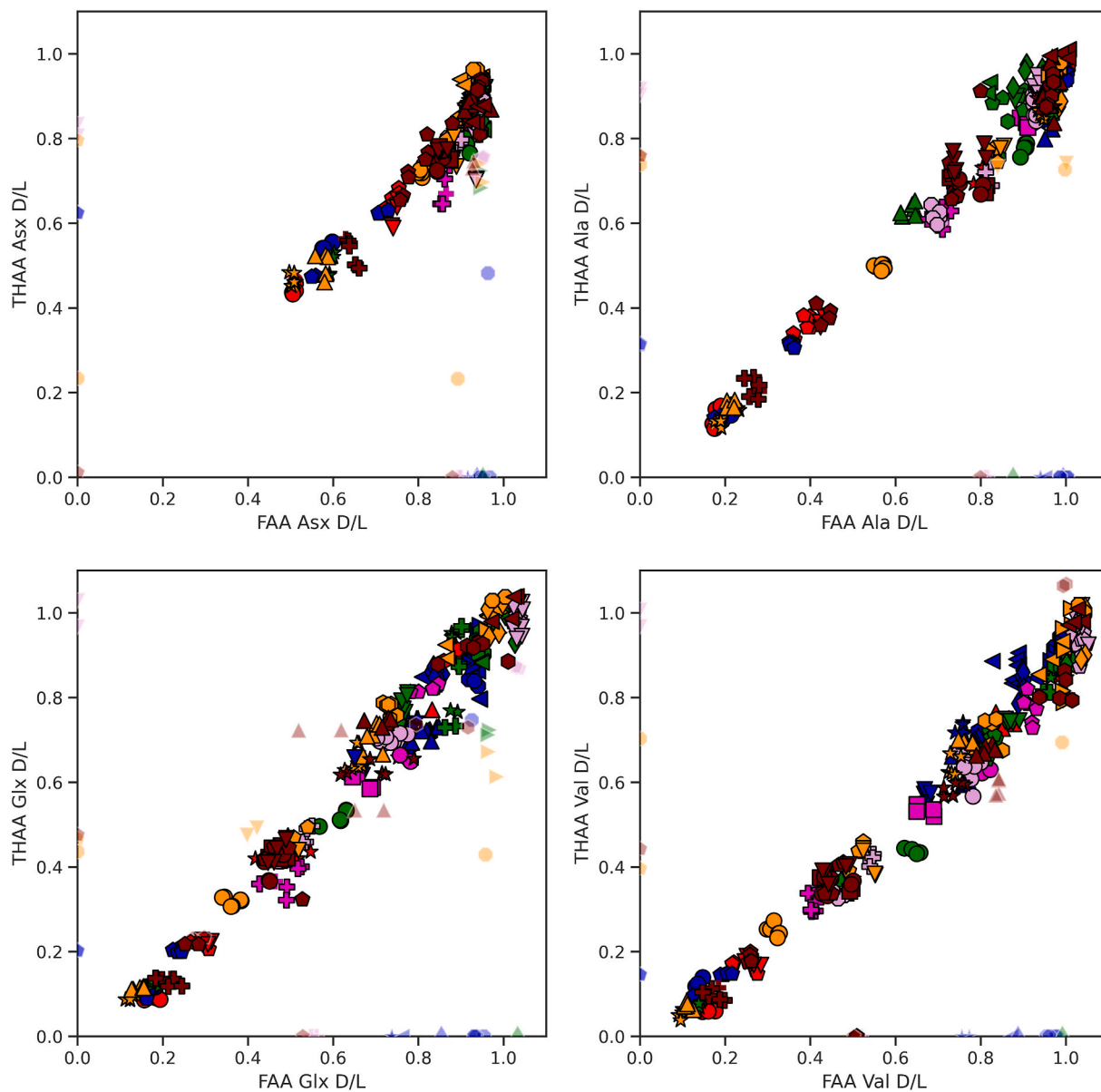
Fig. 5. *Bithynia* opercula IcPD from horizons analysed throughout the seven cores. The FAA and THAA D/L values are plotted against one another; if a closed system has been retained these two fractions should be strongly correlated. The D/L value increases with the age of the sample. Therefore, younger samples plot to the bottom left and older samples to the top right. Outliers that have been removed from the rest of the data analysis are represented by semi-transparent markers.

The relationship between the D/L values and depth between the cores is consistent with their differing sedimentation rates (Fig. 3); for example, the samples from the Makó Trough show lower D/L values than samples with similar depths from the Körös Basin.

3.3. Extent of IcPD with age

To determine how IcPD increases with age, the magnetic susceptibility stratigraphy correlated with the MIS record developed by Püspöki et al. (2021a) was used to define age boundaries throughout each core. The extent of racemisation in both the FAA and THAA fractions increases with the age of the sample (Figs. 7 and 8).

Different amino acids degrade at different rates, so the multiple parameters measured through the IcPD approach provide independent isochronic information. Asx racemises fastest out of the four amino acids discussed here; not only does it racemise rapidly as a free amino acid, but unlike most other amino acids, aspartic acid can racemise whilst still peptide bound (Brennan and Clarke, 1993). As such, it provides good

levels of temporal resolution for the youngest material (Fig. 6; MS 0 to MS 3; ~40–430 ka). In subsequent MS cycles, the extent of racemisation reaches equilibrium and discrimination between older horizons is no longer possible (Figs. 8, A.1 & A.5).

Ala racemises at an intermediate rate, enabling temporal resolution at a range of time scales, and is particularly useful for resolving samples attributed to the Middle Pleistocene (Penkman et al., 2013; Tesakov et al., 2020). In this dataset Ala provides the best resolution from MS 0–4 (~40–950 ka), where the amino acid nears racemic equilibrium (Fig. A.2 & A.6).

Glx and Val are both slow racemising amino acids, extending the resolution in older age material and therefore improving age discrimination within the Early Pleistocene. In this dataset, both amino acids are able to provide age discrimination up to MS 10 (~40 ka – 2.5 Ma). However, due to the slow rates of racemisation, discrimination between samples from horizons correlated to MS 0–2 is poorer compared to the faster racemising amino acids (Val: Fig A.3, A.4, 7 & 8; Glx: A.7 & 8).

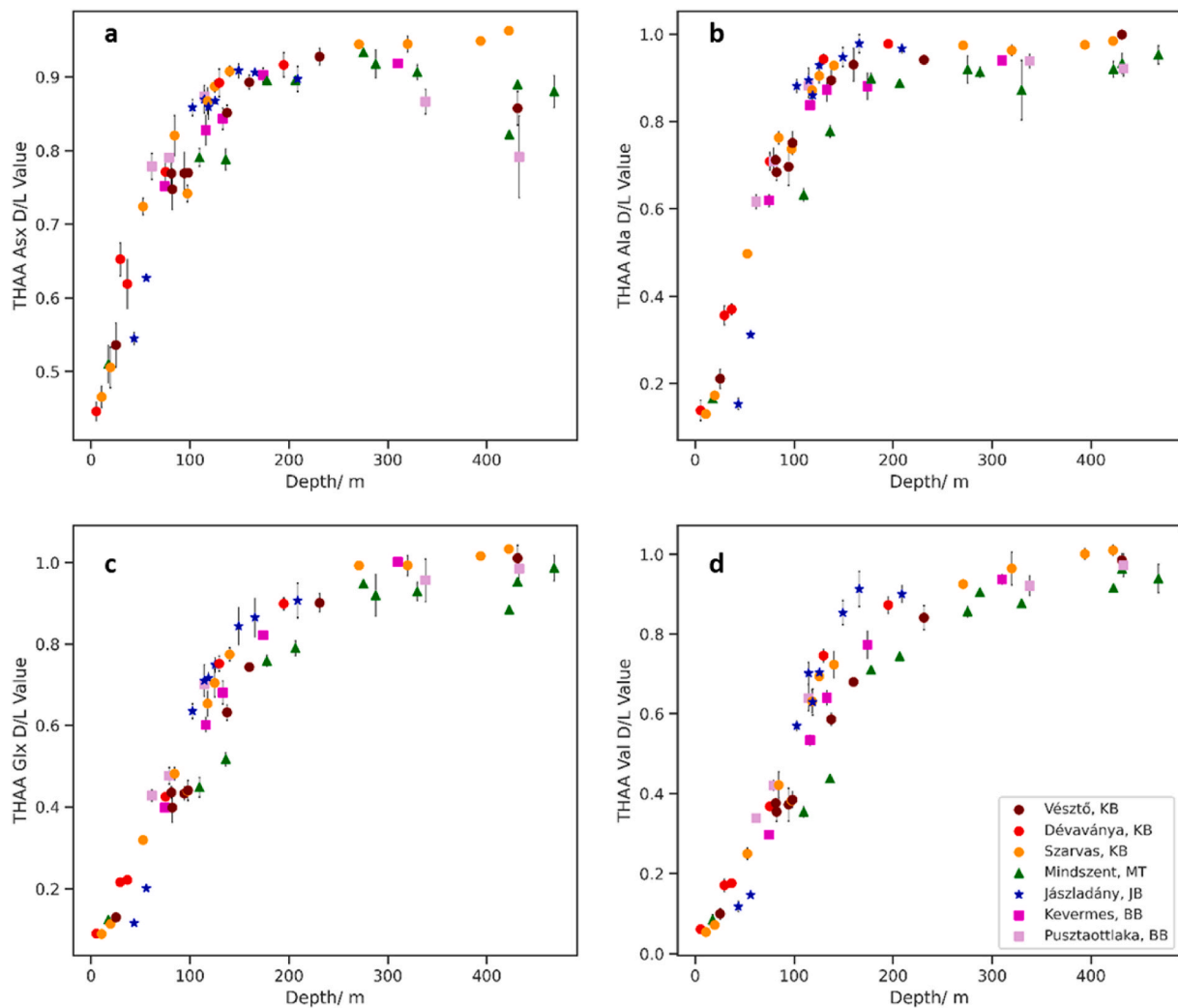Valine is particularly informative for this sample set because the

Fig. 6. The mean THAA D/L value ± 1 σ for each horizon analysed for Asx (a), Ala (b), Glx (c), and Val (d). IcPD increases with depth; in some of the cores and amino acids equilibrium is reached, the depth for which varies between each amino acid (racemising at different rates), and each borehole (differing rates of sedimentation). The different sub-basins have been defined by the following shapes: Körös Basin (KB) = circle, Makó Trough (MT) = triangle, Jászság Basin (JB) = star, Békés Basin (BB) = square.

majority of samples analysed have been attributed to the Middle Pleistocene or Early Pleistocene; therefore, this slower racemising amino acid provides the best temporal resolution for the majority of samples (Figs. 7 and 8).

In the Körös Basin, the most complete record of the Quaternary comes from the Szarvas core. THAA Val reaches racemic equilibrium in Szarvas at 393.75 m (~2366 ka). As there are a greater number of horizons containing opercula in the oldest (MS VII to MS X) section of this core compared to the other cores analysed, the point at which valine racemisation begins to plateau is observable, and occurs in samples deeper than 270 m. This suggests that Val becomes fully racemised in opercula in these deposits by ~2.3 Ma. In Vésztő, the oldest samples from 431.16 m (interpolated age ~2294 ka) have also reached racemic equilibrium. However, there is nearly 1 million years age difference between the oldest sample and the next youngest (231.03 m), so the point at which equilibrium has been reached in this core is unclear. The oldest material recovered from the Dévaványa core comes from MS VI, just below MP 6a (~1358 ka; 194.90–195.28 m), with a mean THAA valine D/L of 0.87 ± 0.01 (n = 4). The D/L value for the same MS cycle from Vésztő (~1289 ka, 231.3–231.78 m) is 0.84 ± 0.03 (n = 4); this suggests that a similar extent of valine racemisation occurs for material of similar age in the Körös Basin cores. In general, THAA Val provides age discrimination for most of the Quaternary in the Körös Basin. Due to

the sparsity of samples greater than 1.2 Ma from Vésztő and Dévaványa, we cannot tell at present if equilibrium is reached at exactly the same time throughout this sub-basin.

However, outside of the Körös Basin, the extent of Val racemisation observed within cores taken from other parts of the Pannonian sub-basins are systematically different. The Mindszent borehole is the sole core analysed from the Makó Trough, where Quaternary sediments reach their deepest extent. In this borehole the extent of Val racemisation is greater than in the Körös Basin cores for sample of apparently the same age. There is a good distribution of opercula samples throughout this borehole, enabling the plateauing of Val racemisation with age to be observed. Val racemisation approaches the plateau by ~1290 ka; at this point temporal resolution between samples begins to decrease. The deepest material is from 468.14 to 469.39 m (interpolated age: ~1769 ka), where valine has become completely racemised in the FAA fraction (1.03 ± 0.01; SI Fig. 3) and is close to racemic equilibrium in the THAA fraction (0.94 ± 0.03). Samples from MS VI in this core (287.69 m, ~1204 ka) have an average D/L value of 0.91 ± 0.01 (n = 4), which is higher than that observed for this MS cycle in the Körös Basin cores. This suggests that IcPD is higher in Mindszent than for equivalent aged samples in the Körös Basin cores.

In the Jászladány core (Jászság Basin), both Val FAA and THAA start to reach equilibrium by ~800 ka (MS IV). The mean THAA Val from
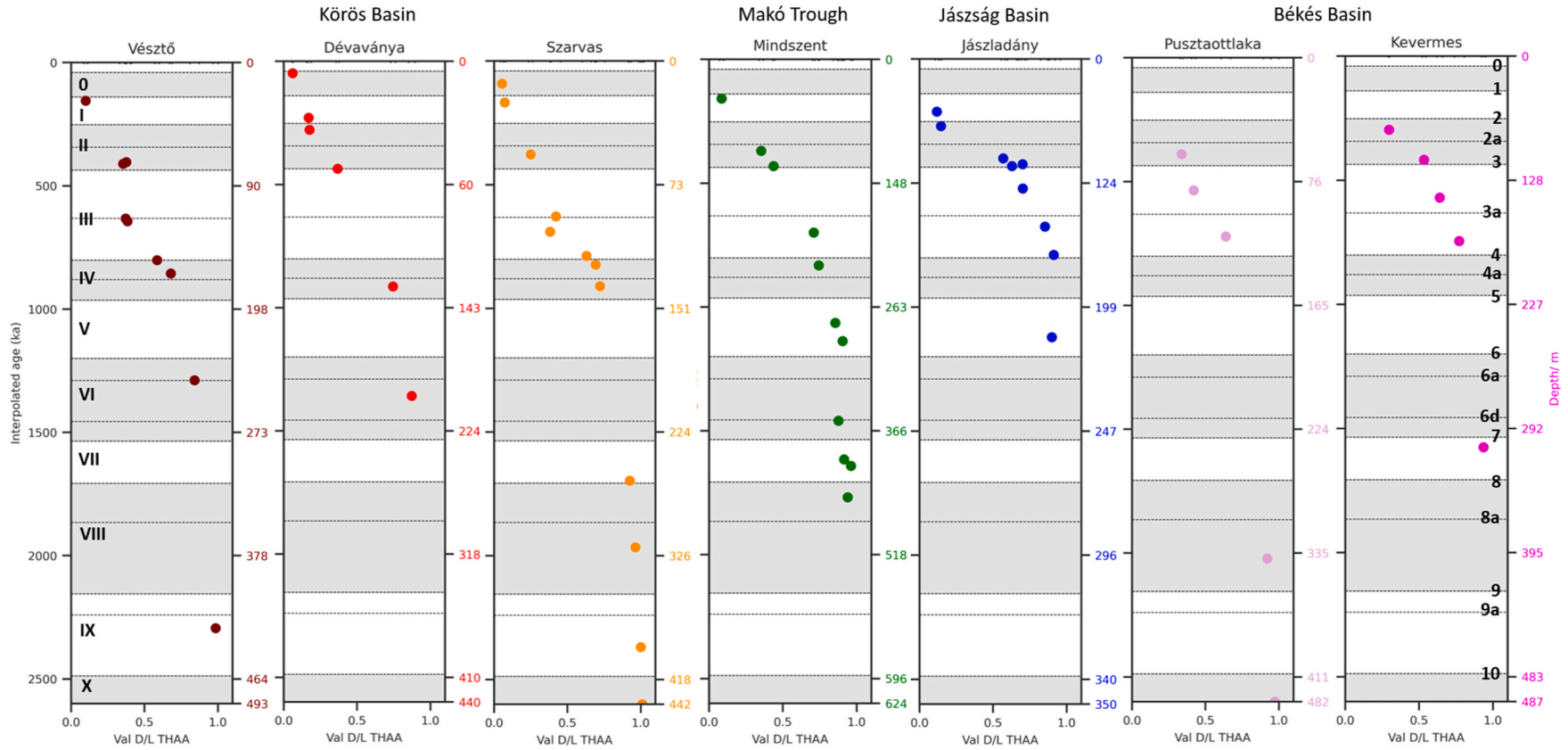
Fig. 7. THAA Val ᴅ/ʟ against both interpolated age (ka; left axis) and depth (m; right axis). The interpolated ages have been modelled based on the position of master peaks within each core and their correlation with the MIS record (Püspöki et al., 2021b). The age of MS cycles (Roman numerals and shading) and master peaks (Arabic numbers and dotted lines) have been presented alongside the ᴅ/ʟ values. The depth of equivalent age sediments is not consistent across the cores. Due to the antiquity of many of the samples analysed here, Val is used to demonstrate the extent of racemisation as it is able to provide age discrimination for Early Pleistocene material. Plots for the other key amino acids can be found in Appendix A Figs A.5-A.7.
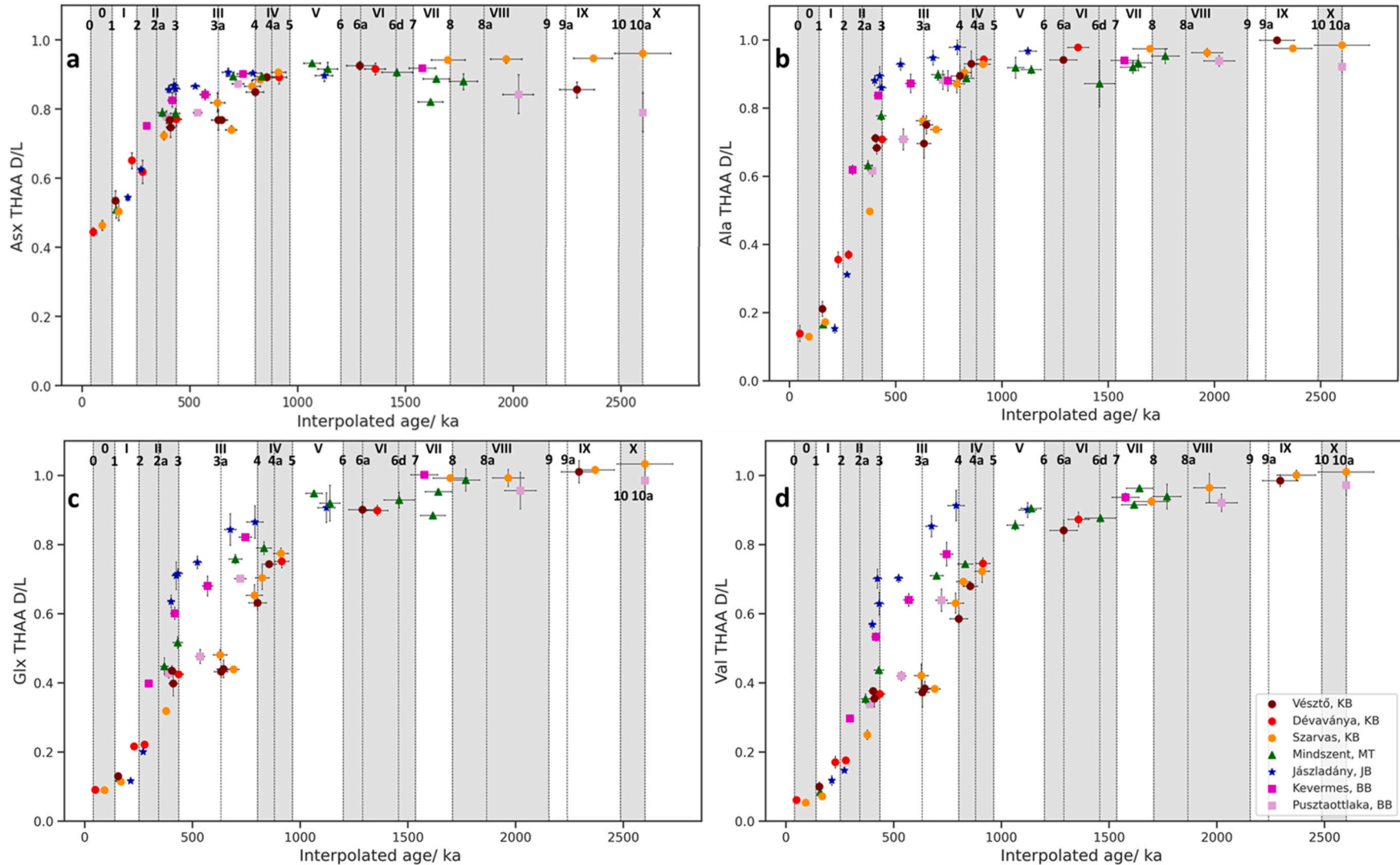
Fig. 8. Comparison of the mean THAA ᴅ/ʟ value of Asx (a), Ala (b), Glx (c), and Val (d) for each horizon vs. the interpolated age of its depth, based on the chronological model developed by Püspöki et al. (2021b). Age boundaries for each master peak are represented by a dotted line. The error in the y axis represents 1 σ about the mean of each horizon, x axis error described in section 2.3. Plots for the FAA fraction can be found in the supplementary material. Note a systematic difference in ᴅ/ʟ values can be observed in different cores prior to ~450 ka until the amino acid starts to reach racemic equilibrium. The different sub-basins have been defined by the following shapes: Körös Basin (KB) = circle, Makó Trough (MT) = triangle, Jászság Basin (JB) = star, Békés Basin (BB) = square.

B. leachii from 165.66 to 165.87 m (MIS III), located just above MP 4 (168 m) is 0.91 ± 0.03 (n = 2), and from 208.85 to 209.03 m (MS V) is 0.90 ± 0.02 (n = 8); older opercula do not occur in this core. Equivalent aged samples from the Körös Basin have substantially lower THAA Val D/L values: in Vésztő THAA Val is 0.58 ± 0.01 (n = 6) at 137.43–138.00 m and at Szarvas THAA Val is 0.63 ± 0.03 (n = 6) at 117.90 m. Similarly to the Mindszent core, IcPD is higher for samples from the Jászladány core attributed to an equivalent age to those from the Körös Basin cores.

In the Békés Basin, the oldest opercula analysed from the Kevermes core are correlated with MS cycle VII (interpolated age: ~1621 ka; 310.00–311.50 m). In these samples, Val is nearing racemic equilibrium, with a D/L value of 0.94 ± 0.01 (n = 4). This is similar to the extent of racemisation observed for samples of equivalent age in the Mindszent core: in Mindszent the THAA Val D/L value is 0.96 ± 0.0 (n = 2) at 431.66 m (~1.6 Ma). In a similarly aged sample from Szarvas (~1.7 Ma) the extent of racemisation is 0.92 ± 0.01 (n = 2). Samples from 432.8 m in the Pusztaottlaka core are of Pliocene age, below the Quaternary deposits. Again, Val has reached racemic equilibrium in both the FAA and THAA fractions (FAA: 1.02 ± 0.01 (n = 4); THAA: 0.97 ± 0.03 (n = 8)). Due to sparsity of samples in both cores, the point at which racemic equilibrium is reached cannot be established for this part of the Pannonian Basin.

In summary, age discrimination can be achieved in all seven of the cores using the slower racemising amino acid, Val, for the majority of the Quaternary. However, IcPD does not increase with age consistently between the cores. In particular, a greater extent of protein decomposition appears to have occurred in Mindszent, Jászladány, and Kevermes when compared to the Körös Basin cores. Similar variation in IcPD with age can be observed in all amino acids analysed. For example, THAA Ala (Figs. 8, A,6) starts to equilibrate around ~800 ka in the Körös Basin cores, before ~700 ka in the Makó trough, and before ~450 ka in the Jászladány and Kevermes core. There is insufficient data from Pusztaottlaka to establish at which point this amino acid starts to equilibrate.

The greatest variation in IcPD occurs between the end of MS cycle II and the end of MS III. Samples located between MS peaks 2a and 3 (estimated age 340–440 ka) occur in all of the cores, and therefore allow a direct comparison of the extent of racemisation. Samples from the Jászladány and Kevermes cores have significantly higher D/L values compared to samples from the other cores. There are also samples from each core, with the exception of Dévaványa, between MS peak 3a and 4 (~632–802 ka). The most racemised samples are those from Jászladány in both instances, followed by Kevermes, and then Mindszent. The least racemised samples attributed to this age ranges come from Pusztaottlaka, Vésztő and Szarvas (the Körös Basin). In samples older than ~1.2 Ma, THAA Val is reaching racemic equilibrium, masking any variation between the cores.

The systematic differences in IcPD between the cores may be due to two factors. The first possibility is that the age model used here does not estimate age accurately for all of the cores. The second is that due to the temperature dependence of the rate of IcPD, equivalent aged deeply-buried opercula samples from different core localities within the Pannonian Basin have not experienced a similar temperature history.

If the original age attribution in the Mindszent, Jászladány, and Kevermes cores is incorrect, the sections of the cores with heightened D/L values have been attributed ~100 ka younger than their true ages. In the Jászladány and Kevermes boreholes, this would indicate that each of the MPs between 100 and 200 m would need to be reassigned to the preceding peak. Should this be the case, this implies that a possible hiatus has occurred at these two localities, resulting in a missing MP peak, leading to an incorrect age attribution of the MS cycles present. In the Mindszent core, the difference in D/L values in comparison to the Körös Basin cores is not so pronounced and a movement of the top of MS cycle IV to incorporate all sand units between 168.6 and 190.6 m would result in a better fit between the previous chronology and the IcPD results, suggesting that all sand units were deposited within the same glacial cycle.

To assess whether the age assignments are incorrect, all evidence constraining the age of this material has been investigated. MS cycle III is a key stratigraphical unit that has multiple lines of evidence to corroborate its assignment to 420–710 ka. Firstly, assessment of palaeomagnetic reversal events within the Dévaványa and Vésztő boreholes by Püspöki et al. (2021a) revealed a number of short-lived polarity reversals and instability events within both the Brunhes and Matuyama epochs. Of particular importance to this section of the core is the Laguna de Sello (343 ka; Channell et al., 2012), West Eifel (583 ka; Bohnel et al., 1987) and Stage 17 (670 ka; Biswas et al., 1999) events which help to constrain the age of the MS III cycle in these two boreholes. In addition to MP 3, the cycle contains diagnostic secondary peaks (3a and b). Magnetic susceptibility can be influenced by various factors (e.g. magnetic minerals becoming concentrated in sediments due to their higher density, or loss of magnetic susceptibility due to weathering), but evidence in the Pannonian Basin suggests that all the fluvial magnetic susceptibility is principally determined by the extension of permafrost zones in the nearby mountainous regions (Püspöki et al., 2021b).

Molluscan biostratigraphic markers also provide constraints on chronology (e.g. Krolopp, 1970, 1995; Meijer, 1988, 2003; Preece et al., 2020). In all three river basins the biostratigraphic marker of the last appearance of *Viviparus boeckhi* (Halaváts, 1888) occurs within the MS cycle III (Püspöki et al., 2016, 2021b). The *V. boeckhi* biozone, an important biostratigraphic marker for this region, was established by Krolopp through the analysis of more than 100 boreholes in the Middle Danube Basin area (Krolopp, 1970; reviewed in Gaudenyi et al., 2013). The *V. boeckhi* zone covers the later part of the Early Cromerian and early Middle Pleistocene (Krolopp, 1970), and is correlated with the Cromerian due to co-occurrence with the rodent *Mimomys savini* (Krolopp, 1970, 2002; Kretzoi and Krolopp, 1972; reviewed in Gaudenyi et al., 2013). The first appearance datum (FADVb) of this species is ~1.1 Ma and last appearance (LADVb) is ~550 ka (Krolopp, 1995, 2014). LADVb has been defined in all cores analysed.

In the Békés Basin, Püspöki et al. (2023) determined the location of the *V. boeckhi* biozone with the support of the other biostratigraphically important fauna present. This includes the presence of *Planorbis planorbis dentata*, a mollusc that occurs concurrently with *V. boeckhi* and *P. crassitesta*, which became extinct at a similar time to the LADVb (Krolopp, 1976). The occurrence of *Melanopsis* sp. and *Dreissena* sp. deeper within the core indicates the occurrence of pre-Quaternary sediments. *P. planorbis dentata* is more widely distributed throughout the Békés Basin cores than *V. boeckhi;* the first and last appearance of this species extends the length of the core attributed to the *V. boeckhi* biozone. Other molluscs provide upper and lower boundaries to this zone.

This combined evidence provides a strong argument that the MP at 116.2 m in the Jászladány core, 135.2 m in the Mindszent core, and 123 m in the Kevermes boreholes should be attributed to MP 3 (~436 ka), and the MP that lies beneath is MP 4 (~802 ka). This therefore suggests that the differences in IcPD between these cores result from differences in their integrated temperature history – that is, that the geothermal conditions in the four sub-regions of the Pannonian Basin studied in this work are not the same. This possibility is investigated in the next section.

3.4. Competing influences on burial temperatures

3.4.1. Geothermal influence on IcPD

Prior to this study, a number of amino acid geochronologies have been developed using material from deep beneath the surface from both marine and terrestrial environments (e.g. Blunt et al., 1981; Katz et al., 1983; Wehmiller and Hall, 1997; Ortiz et al., 2004b; Wheeler et al., 2021; Chauhan et al., 2022). In studies of amino acid decomposition of foraminifera in deep-sea cores, rates of racemisation were found to be higher than those predicted from high temperature experiments (Bada and Luyendyk, 1971; Bada et al., 1974). This was thought to be due to geothermal heating, with the effect predicted to be 10–15 °C of warming by 200 m.b.s.l. (Bada and Man, 1977). However, more recent work has

questioned the applicability of experimental (high) temperature reaction kinetics to natural (ambient) decomposition in some biominerals (e. g. Tomiak et al., 2013; Dickinson et al., 2019; Baldreki et al., 2024). Downcore temperature measurements in a recent study of amino acid decomposition in the North Sea have suggested consistent temperatures in this burial environment (Chauhan et al., 2022), so geothermal heating does not always impact the protein decomposition for deep core material, and will depend on the location of the study. However, given the potential impact on the use of amino acid dating to cross-correlate cores from within the same region (or even further afield), understanding how geothermal conditions effect IcPD is crucial.

To explore the potential for geothermal heating of the samples analysed here, the geothermal gradient for each core was calculated from bottom temperatures from each core and/or boreholes taken within the close vicinity (Fig. 9). Wireline-conveyed maximum recording thermometers and continuous logging tools were used to measure temperatures in the studied boreholes during drilling by continuous coring. In these cases, the warmest thermal data was recorded at the deepest logged point of the wells. To estimate the shallower depth temperatures, additional bottom hole temperature data of the neighbouring shallow wells were taken into consideration. The near surface temperatures estimated for each core are highly uncertain, due to the seasonal variability of temperatures in the first few metres below the surface. The geothermal gradient for each core has been estimated to be: 46.4 °C/km for Dévaványa; 49.4 °C/km for Vésztő; 54.9 °C/km for Szarvas; 40.5 °C/km for Mindszent; 57.4 °C/km for Jászladány; 47.8 °C/km for Pusztaottlaka; and 53.9 °C/km for Kevermes. A typical geothermal gradient for the first 3–5 km of normal continental crust is 25 °C/km (DiPietro, 2013).

The steeper geothermal gradient of the Pannonian Basin occurs due to the extension and thinning of the lithosphere and associated strong warming that occurred during the Middle Miocene (Royden, 1988); resulting in the thickness (60–80 km) of the lithosphere underlying the Miocene-Quaternary basin. In contrast, under the neighbouring Carpathian Mountains and Dinarides the lithosphere is 100–200 km thick (Bielik et al., 2022). In addition, beneath the Pannonian Basin the asthenosphere-lithosphere boundary, whose temperature is 1330 °C (Allen and Allen, 2013), is at a much shallower depth than under the mountain ranges surrounding the basin. Since the Upper Miocene, the
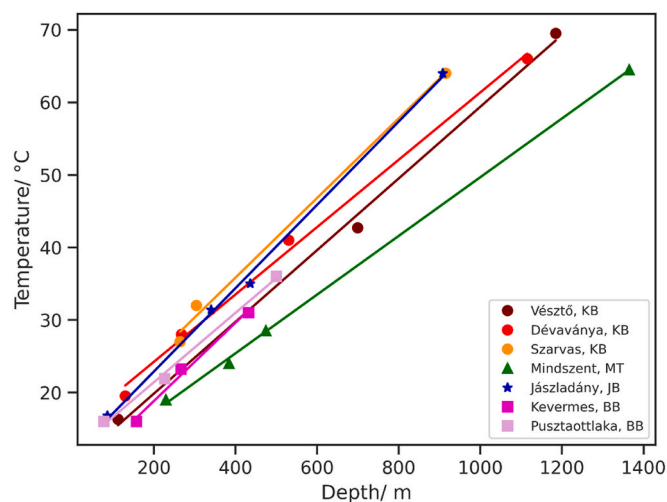
lithosphere of the Pannonian region has been cooling, and different degrees of thermal subsidence has taken place in each sub-basin. However, the heat flow from the depths towards the surface and the geothermal gradient formed in the sediments filling the basin are still much greater today in the Pannonian Basin than under the orogenic mountain ranges surrounding the basin (Lenkey et al., 2021).

The steepest geothermal gradient occurs in the localities of Szarvas and Jászladány, and the flattest in Mindszent. However, the increased trend in IcPD vs age (Fig. 8) occurs within the Jászladány, Kevermes, and Mindszent cores when compared to the Körös Basin cores. Therefore, the geothermal gradient alone does not explain the increase in IcPD within these cores. However, the observed D/L value is not just due to the current temperature each sample is subject to, but its integrated temperature history. Over time samples will be exposed to different temperatures as they become more deeply buried, and the duration they are exposed to various temperatures will vary too.

Therefore, we explored the relationship between depth and temperature against the age of the sample. To do this, the geothermal effect (ΔT) was calculated by multiplying the depth of the sample by the slope of the geothermal gradient estimated for the locality of each core. This was then plotted against the interpolated age of the sample (Fig. 10).

The geothermal effect (ΔT) on samples of the same age is not consistent across the Pannonian Basin (Fig. 10a), as the sedimentation rate varies both temporally and spatially (Fig. 3). Sedimentation has not been uniform across the Pannonian Basin. This means that sediments equivalent in age are at different depths in the sediment columns in different localities, and therefore have been exposed to different temperatures over time. As such, depth and sample age are not the only driver for the extent of racemisation observed in each sample. For example, sediments attributed to 500 ka within the Mindszent core are found at a depth of 148 m, whereas in the Dévaványa core they are found at 77 m; the corresponding ΔT is 6 °C and 3.6 °C, respectively (see Table 3, Fig. 11). A 3-dimensional version of Fig. 10 plotting THAA Val against age and ΔT is available online; the deviation in the trend of D/L values can be seen more clearly, with samples experiencing a greater geothermal effect having a higher D/L value compared to those of the same age that experienced a lower geothermal effect (see Fig. 12).

For Jászladány, Mindszent and Kevermes, there is a significant increase in ΔT compared to the other cores for samples dated to >450 ka. For samples >900 ka there appears to be a smaller difference; however, due to a sparsity of samples attributed to ages greater than this, the differences in the geothermal effect on the thermal conditions of each sample are not as clear. This trend is similar to that observed in the extent of IcPD against interpolated age (Fig. 8).

This systematic difference in THAA Val D/L values is not observed in samples <450 ka. A possible explanation for this is that in general samples <450 ka in age are buried more closely to the surface (<80 m), and therefore their integrated temperature will likely have been more strongly influenced by the climate than geothermal temperatures (Fig. 2). As all seven cores are from the same relatively small geographical region, it is likely there has been no significant difference in the regional climate between the core locations, and therefore all shallowly buried samples will have experienced a more similar temperature history. Those >450 ka are deeply buried enough for differences in geothermal conditions to affect the extent of IcPD.

Here we have demonstrated that in "geothermally hot" regions such as the Pannonian Basin that the sedimentation rate and thermal maturity of the samples will influence IcPD values. This highlights the importance of understanding both the sedimentation history and geothermal conditions of material taken from deep-cores for future amino acid dating studies. Where downcore temperature measurements are available, a correction factor could be developed for the ΔT to directly compare D/L values across the cores with different thermal histories. It is also possible that the kinetics of protein decomposition for material buried deeper underground under more constant temperatures may be more accurately described by high temperature experiments; future work should
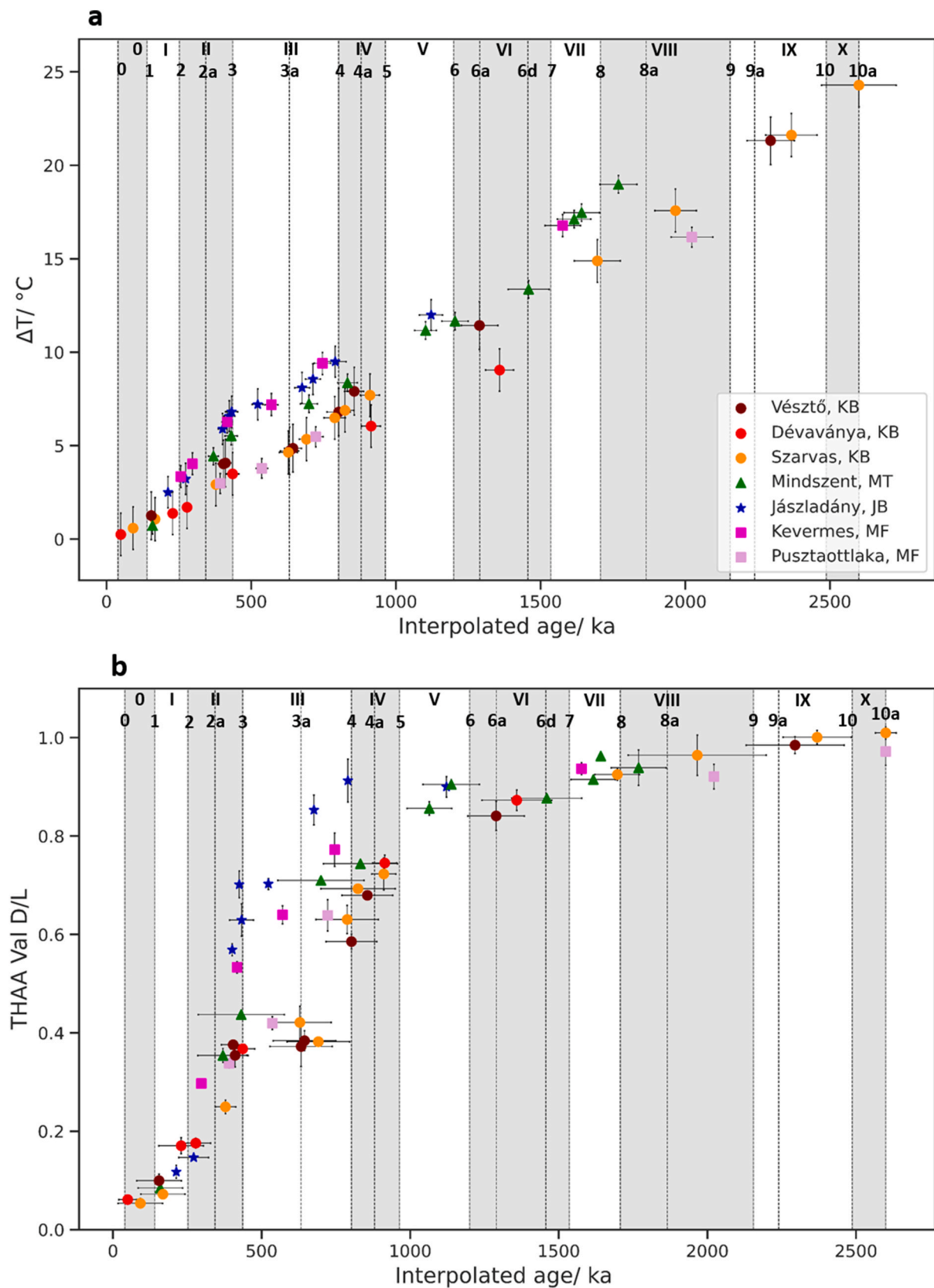

Fig. 9. Geothermal gradient based on bottom temperatures measured in the sampled boreholes and their close vicinity. Each point represents the temperature at the depth it was measured. The calculated gradient has been used to determine the geothermal effect on the temperature at the depths at which the samples were taken. The different sub-basins have been defined by the following shapes: Körös Basin (KB) = circle, Makó Trough (MT) = triangle, Jászság Basin (JB) = star, Békés Basin (BB) = square.

Fig. 10. The relationship between geothermal effect (ΔT (a); the change in temperature with age of the sample due to the geothermal gradient for each core location) and the interpolated age of the samples for each core. ΔT y axis error is the 1 σ of the mean squared error of the linear regression model calculated in Fig. 9 (b): Fig. 8, THAA Val D/L vs. interpolated age has been repeated here for direct comparison to the change in ΔT with age. An interactive 3D plot of age (ka) and THAA Val D/L vs. ΔT (°C) is available online. Samples from Kevermes, Jászladány and Mindszent are warmer for a given age and D/L value. The different sub-basins have been defined by the following shapes: Körös Basin (KB) = circle, Makó Trough (MT) = triangle, Jászság Basin (JB) = star, Békés Basin (BB) = square.

Table 3

A comparison of the depth and geothermal effect (ΔT) of sediments attributed to 500 ka from each borehole along with an interpolated mean THAA Val D/L. Deeper sediments experience a greater geothermic effect and this results in higher IcPD. The warmer layers are highlighted in bold.

Borehole	Depth/ m	Geothermal effect (ΔT)/ °C	Est. mean THAA Val D/L
Vésztő	90	4.4	0.37 ± 0.001
Dévaványa	77	3.6	0.38 ± 0.004
Szarvas	73	4.2	0.36 ± 0.009
Mindszent	**148**	**6.0**	**0.52 ± 0.020**
Jászladány	**124**	**7.1**	**0.69 ± 0.011**
Pusztaottlaka	75	3.6	0.40 ± 0.009
Kevermes	**127**	**7.0**	**0.61 ± 0.009**
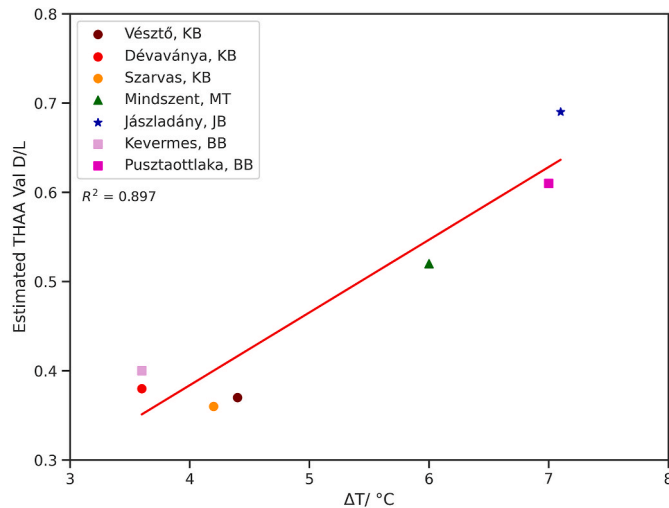
Fig. 11. The estimated geothermal effect (ΔT/°C) vs. the interpolated THAA Val D/L values for sediments attributed to 500 ka. These two variables are highly correlated ($R^2 = 0.897$), supporting the conclusion that a greater geothermal effect due to sediments being more deeply buried has affected the extent of protein decomposition within a sample. The different sub-basins have been defined by the following shapes: Körös Basin = circle, Makó Trough = triangle, Jászság Basin = star, Békés Basin = square.

explore this.

3.4.2. Surface climate vs. geothermal influence on IcPD

The other parameter that can affect the integrated temperature history experienced by fossils is surface climate. Today, the climate throughout the European continent varies from oceanic, temperate conditions in the west, Mediterranean conditions to the south and more continental conditions to the east (Pajek et al., 2019). Modern-day mean annual temperatures range from 2.2 °C in Norway to 19.6 °C in Malta (average mean surface temperature, 1991–2020; Harris et al., 2020). Regional climate and temperature have varied throughout the

Table 4

The modern-day temperatures between the European regions compared in this study are presented in the table below. This includes the mean surface temperature between 1991 and 2020; mean winter temperature (December–February), and mean summer temperature (June–July; Harris et al., 2020).

Region	Mean surface temperature (1991–2020)/° C	Mean winter (DJF) surface temperature (1991–2020)/° C	Mean summer (JJA) surface temperature (1991–2020)/° C
Hungary	11.5	0.9	21.5
England	9.1	4.7	15.8
The Netherlands	10.5	3.9	17.4
EEP	7–11	-3-[+]1	20–23

Quaternary, and will have influenced the rate of protein decomposition in fossils buried close to the surface during that time. Given their proximity, the difference in surface temperatures in these cores throughout the Quaternary will have been minimal. Therefore, to assess the impact geothermal temperatures have on IcPD, the amino-stratigraphy developed for the Pannonian Basin has been compared to datasets developed using shallow bithyniid opercula material for other regions.

Previously published aminostratigraphies (Fig. 12) have been developed for the UK and the Netherlands (Penkman et al., 2011, 2013; Preece et al., 2020) and the East European Plain (EEP; Tesakov et al., 2020). The UK and the Netherlands currently have oceanic temperate climates, with cool, wet winters and warm, wet summers. The EEP is more continental, with more extremes in temperatures between summer and winter (Beck et al., 2018; European Environment Agency, 2012). The Pannonian Basin is at a boundary between the more humid conditions of western Europe, the Mediterranean climate to the south, and continental climate to the east (European Environment Agency, 2007). Modern mean surface temperatures for each region is presented in Table 4 to provide an indication of the temperature difference between these regions.

The extent of racemisation in samples younger than ~500 ka follows a similar trend in the Hungarian data to previously published IcPD datasets. The samples from the UK, Netherlands and EEP were all recovered from depths of less than 60 m, so temperature histories are likely a result of climatic variation rather than geothermal conditions. Samples attributed to less than ~500 ka from Hungary were also found at depths of less than 70–100 m, so the integrated temperature experienced will likely be strongly influenced by the climate as well. The data from the Pannonian Basin starts to deviate from the other regions ~600 ka, with significantly higher D/L values in the Pannonian Basin cores. In the UK and Dutch aminostratigraphy, Val can be used to discriminate between Early Pleistocene and Pliocene deposits (Penkman et al., 2013; Preece et al., 2020); in the EEP racemic equilibrium in THAA Ala is reached by 1.8 Ma, while THAA Val is not fully racemised by ~2.6 Ma. Based on modern day temperatures (Table 4) and climate, it is likely that temperatures were similar in Hungary to the EEP, and therefore should climate be the sole influence on temperature a similar trend in D/L values could be expected between the two regions. In comparison, valine has become fully racemised by ~2.3 Ma in the Hungarian material. Similar trends in the first 500 ka in IcPD suggests that the differences in the deeper material are unlikely to be due only to climatic differences between Hungary and the rest of Europe. This therefore supports the systematic increase in protein decomposition due to geothermal heating in deeper samples from the Pannonian Basin in comparison to other European material analysed.

Comparing these datasets shows how significant an effect the burial depth and geothermal heating has had on the extent of racemisation in the opercula from the Pannonian Basin cores. It is likely that a combination of the loss of the influence of the surface climate from above, and an increase in the influence of geothermal heating from below, have both resulted in a greater overall extent of protein decomposition compared to samples recovered from nearer the surface. However, we have only looked at long cores from one region in this study; additional long core material from other regions is needed to determine whether this is the case more broadly.

4. Conclusions

Bithyniid opercula from seven fully-cored boreholes from the Pannonian Basin, Hungary, were sampled and analysed for IcPD. This was the first study to test the ability of IcPD to date terrestrial material from sediments located deeper than 63 m below the surface, with opercula recovered from depths between ~5 and 470 m. The level of protein decomposition observed increased with the depth of the sample in all cores. Racemic equilibrium was not reached in the slowest racemising
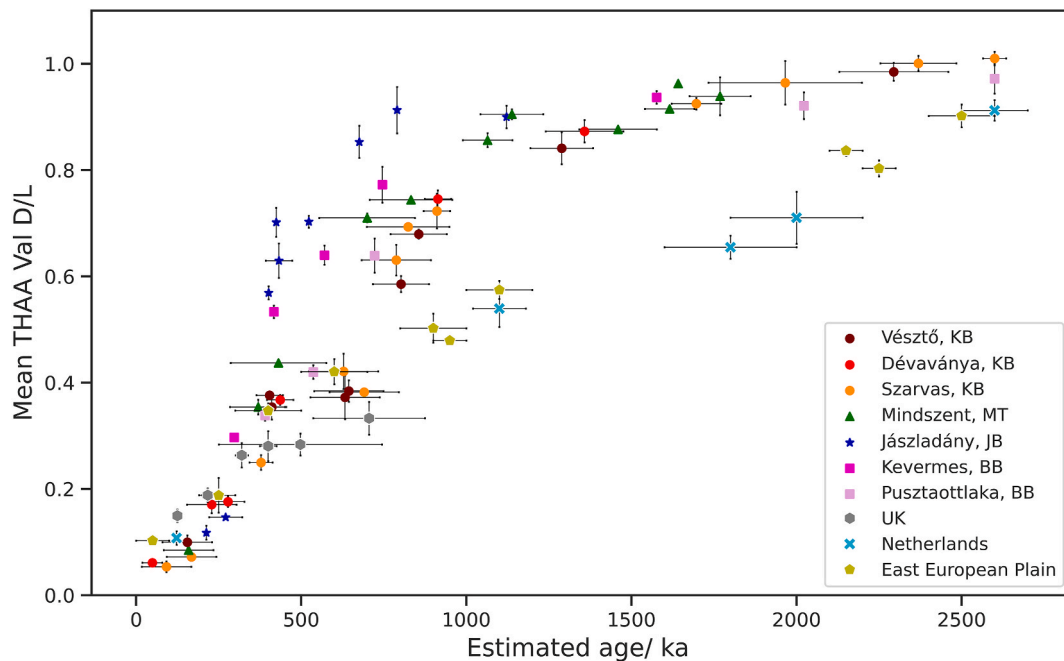
Fig. 12. The Pannonian Basin aminostratigraphy compared to aminostratigraphies for the UK (Penkman et al., 2011, 2013), Netherlands (Preece et al., 2020), and East European Plain (Tesakov et al., 2020). Estimated ages are plotted with their mid-point and potential age range as x-axis error bars; for the Pannonian Basin these are estimated using the Monte Carlo approach, whereas for the other regions they encompass the potential age range given current understanding. For example, sites attributed to the Cromerian are centred at 650 ka, with x-error bars extending the whole range of the Cromerian interval. The different sub-basins in Hungary have been defined by the following shapes: Körös Basin = circle, Makó Trough = triangle, Jászság Basin = star, Békés Basin = square.

amino acids until the deepest part of the cores, up to ~2.3 Ma. The IcPD results support the cross-correlations made between these boreholes by Püspöki et al. (2016, 2020, 2021a, 2021b, 2023) using cycles of magnetic susceptibility in most instances. In addition, this work demonstrates the ability of IcPD to provide chronological information for long core material for the majority of the Quaternary even in regions that are geothermally hot. This is particularly important for deposits beyond the range of other dating methods, such as luminescence or radiocarbon dating.

The rate of IcPD was greater between MS cycle II and MS cycle V for material from the Jászladány, Kevermes and Mindszent boreholes, compared to the palaeomagnetically dated boreholes from the Körös Basin. This difference was not observed in younger material, or in material approaching racemic equilibrium, where the ability to discriminate between different ages and levels of protein decomposition becomes challenging. This indicated that either the original age attribution for the cores with systematically higher D/L values was incorrect, or these opercula had been exposed to higher temperatures. An incorrect age attribution is unlikely as other independent evidence of age supports the existing age-model. The differences in IcPD can be explained by the relationship between the age, depth and temperature of the sample. Samples of equivalent age that were buried more deeply underground would have been exposed to a greater extent of warming from geothermal heating than those buried closer to the surface, increasing the IcPD in these deeper samples. This resulted in equivalently-aged samples from the Kevermes, Jászladány and Mindszent cores having higher IcPD compared to the cores from the Körös Basin and the Pusztaottlaka core.

Hungarian samples older than around ~600 ka had higher IcPD compared to equivalently aged samples from the UK, Netherlands and EEP. This could be due to a combination of a loss of the influence of surface climate in material of this age from Hungary, and increased geothermal heating of samples in this region. An understanding of how these two competing factors affect IcPD would support not only cross-correlation of material with different thermal maturities within the

Pannonian Basin region, but also help with correlations of IcPD results between regions which have experienced different temperature histories. This work highlights the importance in understanding the temperature environment of the material used when creating a regional aminostratigraphy to correlate different horizons in deeply buried material. Where possible, downcore temperature measurements should be made for studies of this nature. Future work should continue to explore how geothermally active regions can affect the extent of protein decomposition for amino acid dating, and investigate the use of a correction factor to cross-correlate between cores with different thermal histories.

CRediT authorship contribution statement

Declaration of competing interest

Appendix A. Supplementary data

Supplementary data to this article can be found online at https://doi.org/10.1016/j.quascirev.2024.109044.

Data availability

Data in this study has been included in the supplementary information and will be available on the NOAA data repository: https://www.ncei.noaa.gov/pub/data/paleo/aar/.

References

Allen, P.A., Allen, J.R., 2013. Basin Analysis: Principles and Application to Petroleum Play Assessment, third ed. Wiley-Blackwell, Chichester, West Sussex, UK.

Bada, J.L., Luyendyk, B.P., 1971. Response: a route to late Cenozoic temperature history? Science 172, 503. https://doi.org/10.1126/science.172.3982.503.b.

Bada, J.L., Schroeder, R.A., Carter, G.F., 1974. New evidence for the antiquity of man in North America deduced from aspartic acid racemization. Science 184, 791–793. https://doi.org/10.1126/science.184.4138.791.

Bada, J.L., Man, E.H., 1977. Initial reports of the Deep Sea Drilling Project, 37. In: Initial Reports of the Deep Sea Drilling Project. U.S. Government Printing Office. https://doi.org/10.2973/dsdp.proc.37.1977.

Bada, J.L., Shou, M.-Y., Man, E.H., Schroeder, R.A., 1978. Decomposition of hydroxy amino acids in foraminiferal tests; kinetics, mechanism and geochronological implications. Earth Planet Sci. Lett. 41, 67–76. https://doi.org/10.1016/0012-821X(78)90042-0.

Bada, J.L., Wang, X.S., Hamilton, H., Amber, R.P., Finch, P., Grocke, D.R., Eglinton, G., Macko, S.A., 1999. Preservation of key biomolecules in the fossil record: current knowledge and future challenges (and discussion). Phil. Trans. Roy. Soc. Lond. B 354, 77–87.

Baldreki, C., Burnham, A., Conti, M., Wheeler, L., Simms, M.J., Barham, L., White, T.S., Penkman, K., 2024. Investigating the potential of African land snail shells (Gastropoda: Achatininae) for amino acid geochronology. Quat. Geochronol. 79, 101473. https://doi.org/10.1016/j.quageo.2023.101473.

Bates, M.R., 1993. Quaternary aminostratigraphy in Northwestern France. Quat. Sci. Rev. 12, 793–809. https://doi.org/10.1016/0277-3791(93)90018-H.

Beaulieu, J.-L. de, Reille, M., 1992. Long Pleistocene pollen sequences from the Velay Plateau (Massif Central, France). Veg. Hist. Archaeobotany 1, 233–242. https://doi.org/10.1007/BF00189500.

Beck, H.E., Zimmermann, N.E., McVicar, T.R., Vergopolan, N., Berg, A., Wood, E.F., 2018. Present and future Köppen-Geiger climate classification maps at 1-km resolution. Sci. Data 5, 180214. https://doi.org/10.1038/sdata.2018.214.

Bielik, M., Zeyen, H., Starostenko, V., Makarenko, I., Legostaeva, O., Savchenko, S., Dérerova, J., Grinc, M., Godová, D., Pánisová, J., 2022. A review of geophysical studies of the lithosphere in the Carpathian-Pannonian Region. Geol. Carpathica 73 (6), 499–516. https://doi.org/10.31577/GeolCarp.73.6.2.

Biswas, D.K., Hyodo, M., Taniguchi, Y., Kaneko, M., Katoh, S., Sato, H., Kinugasa, Y., Mizuno, K., 1999. Magnetostratigraphy of Plio-Pleistocene sediments in a 1700-m core from Osaka Bay, southwestern Japan and short geomagnetic events in the middle Matuyama and early Brunhes chrons. Palaeogeogr. Palaeoclimatol. Palaeoecol. 148, 233–248. https://doi.org/10.1016/S0031-0182(98)00185-0.

Blunt, D.J., Kvenvolden, K.A., Sims, J.D., 1981. Geochemistry of amino acids in sediments from Clear Lake, California. Geology 9, 378–382. https://doi.org/10.1130/0091-7613(1981)9<378:GOAAIS>2.0.CO;2.

Bodri, L., 1981. Geothermal model of the earth's crust in the Pannonian basin. Tectonophysics 72, 61–73. https://doi.org/10.1016/0040-1951(81)90087-1.

Bohnel, H., Reismann, N., Jager, G., Haverkamp, U., Negendank, J.F.W., Schmincke, H.-U., 1987. Paleomagnetic investigation of Quaternary West Eifel volcanics (Germany): indication for increased volcanic activity during geomagnetic excursion/event? J. Geophys. 62, 50–61.

Boyer, P.D., Lardy, H.A., Myrbäck, 1959. The Enzymes.

Brennan, T.V., Clarke, S., 1993. Spontaneous degradation of polypeptides at aspartyl and asparaginyl residues: effects of the solvent dielectric. Protein Sci.: A Publication of the Protein Society 2, 331–338. https://doi.org/10.1002/pro.5560020305.

Brooks, A.S., Hare, P.E., Kokis, J.E., Miller, G.H., Ernst, R.D., Wendorf, F., 1990. Dating Pleistocene archaeological sites by protein diagenesis in ostrich eggshell. Science 248, 60–64. https://doi.org/10.1126/science.248.4951.60.

Channell, J.E.T., Hodell, D.A., Curtis, J.H., 2012. ODP site 1063 (Bermuda rise) revisited: oxygen isotopes, excursions and paleointensity in the Brunhes chron. G-cubed 13, 2011GC003897. https://doi.org/10.1029/2011GC003897.

Chauhan, T., Sejrup, H.P., Hjelstuen, B.O., Kaufman, D.S., Baig, I., Reinardy, B.T.I., 2022. Chronology of early to Mid-Pleistocene sediments in the northern North Sea: new evidence from amino acid and strontium isotope analyses. Quat. Geochronol., 101336 https://doi.org/10.1016/j.quageo.2022.101336.

Cooke, H.B.S., Hall, J.M., Rónai, A., 1979. Paleomagnetic sedimentary and climactic records from boreholes at Dévaványa and Vésztő, Hungary. Acta Geol. Acad. Sci. Hung. 22, 89–109.

Dickinson, M.R., Lister, A.M., Penkman, K.E.H., 2019. A new method for enamel amino acid racemization dating: A closed system approach. Quaternary Geochronology 50, 29–46. https://doi.org/10.1016/j.quageo.2018.11.005.

Ding, Z.L., Derbyshire, E., Yang, S.L., Sun, J.M., Liu, T.S., 2005. Stepwise expansion of desert environment across northern China in the past 3.5 Ma and implications for monsoon evolution. Earth Planet Sci. Lett. 237, 45–55. https://doi.org/10.1016/j.epsl.2005.06.036.

DiPietro, J.A., 2013. Chapter 20 - keys to the interpretation of geological history. In: DiPietro, J.A. (Ed.), Landscape Evolution in the United States. Elsevier, Boston, pp. 327–344. https://doi.org/10.1016/B978-0-12-397799-1.00020-8.

European Environment Agency, 2007. Europe's biodiversity — biogeographical regions and seas: biogeographical regions in Europe: the Pannonian region — the remains of the Pannonian Sea. Original contributions from ETC/NPB: Sophie Condé, Dominique Richard (coordinators). In: Liamine, Nathalie (Ed.), Anne-Sophie Leclère (Data Collection and Processing), Barbara Sotolargo (Drafting), Ulla Pinborg (Final Co-editor). Map Production: UNEP/GRID Warsaw (final Production). Project Manager: Tor-Björn Larsson, EEA. ZooBoTech HB, Sweden, Linus Svensson (Final Edition). European Environment Agency, Copenhagen.

European Environment Agency, 2012. Main Climates of Europe. European Environment Agency. Available at: https://www.eea.europa.eu/data-and-maps/figures/climate. (Accessed 19 June 2024).

Follieri, M., Magri, D., Sadori, L., 1989. Pollen stratigraphical synthesis from Valle di Castiglione (Roma). Quat. Int. 3–4, 81–84. https://doi.org/10.1016/1040-6182(89)90076-1t.

Franyó, F., 1992. Quaternary Isopach Map of Hungary. 1:200 000. SARA datastore.

Gábris, G., Nádor, A., 2007. Long-term fluvial archives in Hungary: response of the Danube and Tisza rivers to tectonic movements and climatic changes during the Quaternary: a review and new synthesis. Quat. Sci. Rev. 26, 2758–2782.

Gaudenyi, T., Nenadić, D., Jovanović, M., Bogićević, K., 2013. The stratigraphical importance of the *Viviparus boeckhi* Horizon of Serbia. Quaternary International, Pan-European Correlations in Quaternary Stratigraphy: SEQS 2011, INQUA Congress, Bern 292, 101–112. https://doi.org/10.1016/j.quaint.2012.11.034.

Gibbard, P.L., Hughes, P.D., 2021. Terrestrial stratigraphical division in the Quaternary and its correlation. J. Geol. Soc. 178. https://doi.org/10.1144/jgs2020-134.

Goodfriend, G.A., 1989. Complementary use of amino-acid epimerization and radiocarbon analysis for dating of mixed-age fossil assemblages. Radiocarbon 31, 1041–1047. https://doi.org/10.1017/S0033822200012698.

Goodfriend, G.A., 1991. Patterns of racemization and epimerization of amino acids in land snail shells over the course of the Holocene. Geochem. Cosmochim. Acta 55, 293–302. https://doi.org/10.1016/0016-7037(91)90418-5.

Haas, J., Budai, T., Csontos, L., Fodor, L., Konrad, G., Koroknai, B., 2014. Geology to the pre-Cenozoic basement of Hungary. Explanatory notes of the "Pre-Cenozoic geological map of Hungary 1, 500000.

Harris, I., Osborn, T.J., Jones, P., Lister, D., 2020. Version 4 of the CRU TS monthly high-resolution gridded multivariate climate dataset. Sci. Data 7, 109. https://doi.org/10.1038/s41597-020-0453-3.

Halaváts, J., 1888. Der artesische Brunnen von Szentes. Mitteilungen aus dem Jahrbuche der königlichen ungarischen Geologischen Reichsanstalt 8, 165–194.

Häuselmann, Ph, Fiebig, M., Kubik, P.W., Adrian, H., 2007. A first attempt to date the original "Deckenschotter" of Penck and Brückner with cosmogenic nuclides. Quaternary International, From the Swiss Alps to the Crimean Mountains - Alpine Quaternary stratigraphy in a European context 164–165 33–42. https://doi.org/10.1016/j.quaint.2006.12.013.

Hearty, P.J., Aharon, P., 1988. Amino acid chronostratigraphy of late Quaternary coral reefs: Huon Peninsula, New Guinea, and the Great Barrier Reef, Australia. Geology 16, 579–583. https://doi.org/10.1130/0091-7613(1988)016<0579:AACOLQ>2.3.CO;2.

Hill, R.L., 1965. Hydrolysis of proteins. In: Advances in Protein Chemistry. Elsevier, pp. 37–107. https://doi.org/10.1016/S0065-3233(08)60388-5.

Horváth, F., Cloetingh, S., 1996. Stress-induced late-stage subsidence anomalies in the Pannonian basin. Tectonophysics, Dynamics of Extensional Basins and Inversion. Tectonics 266, 287–300. https://doi.org/10.1016/S0040-1951(96)00194-1.

Horváth, F., Musitz, B., Balázs, A., Végh, A., Uhrin, A., Nádor, A., Koroknai, B., Pap, N., Tóth, T., Wórum, G., 2015. Evolution of the Pannonian basin and its geothermal resources. Geothermics 53, 328–352. https://doi.org/10.1016/j.geothermics.2014.07.009.

Hungarian Meteorological Service, 2024. Precipitation in Hungary. Hungarian Meteorological Service. (Accessed 23 October 2024).

Kalos, M.H., Whitlock, P.A., 2009. Monte Carlo Methods, second ed. Wiley, Hoboken.

Katz, B.J., Harrison, C.G.A., Man, E.H., 1983. Geothermal and other effects on amino acid racemization in selected Deep-Sea Drilling Project cores. Org. Geochem. 5, 151–156. https://doi.org/10.1016/0146-6380(83)90025-6.

Kaufman, D.S., Manley, W.F., 1998. A new procedure for determining DL amino acid ratios in fossils using reverse phase liquid chromatography. Quat. Sci. Rev. 17, 987–1000. https://doi.org/10.1016/S0277-3791(97)00086-3.

Knudsen, K.L., Sejrup, H.P., 1988. Amino acid geochronology of selected interglacial sites in the North Sea area. Boreas 17, 347–354. https://doi.org/10.1111/j.1502-3885.1988.tb00967.x.

Kosnik, M.A., Kaufman, D.S., 2008. Identifying outliers and assessing the accuracy of amino acid racemization measurements for geochronology: II. Data screening. Quat. Geochronol. 3, 328–341. https://doi.org/10.1016/j.quageo.2008.04.001.

Kossiakoff, A.A., 1988. Tertiary structure is a principal determinant to protein deamidation. Science 240, 191–194. https://doi.org/10.1126/science.3353715.

Kretzoi, M., Krolopp, E., 1972. Oberpliozäne und quartäre Stratigraphie des Alföld (Grosse Ungarischen Tiefbene) aufgrund paläontologischen Angaben. Foldr. Ertesito 21, 133–158.

Krolopp, E., 1970. Őslénytani adatok a nagyalföldi pleisztocén és felsőpliocén rétegek sztratigráfiájához [Contribution to the stratigraphy of the Pleistocene and Upper Pliocene deposits of the Great Hungarian Plain]. Oslenytani Vitak (Discuss. Palaeontol.) 14, 5–39.

Krolopp, E., 1976. Felkérés amalakológus kollégákhoz. Soosiana 4, 44.

Krolopp, E., 1995. Biostratigraphic division of Pleistocene formations in Hungary, according to their mollusc fauna. In: Füköh, L. (Ed.), Quaternary Malacostratigraphy in Hungary, Malacological Newsletter, vol. 1, pp. 17–78. Supplement.

Krolopp, E., 2002. Lower Pleistocene mollusc fauna from the borehole gorgeteg-I SW Hungary also-pleisztocen Mollusca-fauna a gorgeteg-I furasbol. Foldtani Kozlony 1321, 89–94.

Krolopp, E., 2014. Taxonomic, faunistic, stratigraphic and paleoecological evaluation of the Hungarian Pleistocene mollusc fauna. Malacological Newsletter 31, 4–57.

Leeuw, N.H. de, Parker, S.C., 1998. Surface structure and morphology of calcium carbonate polymorphs calcite, aragonite, and vaterite: an atomistic approach. J. Phys. Chem. B 102, 2914–2922. https://doi.org/10.1021/jp973210f.

Lenkey, L., Mihályka, J., Paróczi, P., 2021. Review of geothermal conditions of Hungary. Foldtani Kozlony 151 (1), 65–78. https://doi.org/10.23928/foldt.kozl.2021.151.1.65.

Lisiecki, L.E., Raymo, M.E., 2005. A Pliocene-Pleistocene stack of 57 globally distributed benthic δ^{18}O records: Pliocene-Pleistocene benthic stack. Paleoceanography 20, PA1003. https://doi.org/10.1029/2004PA001071.

Meijer, T., 1988. Mollusca from the borehole Zuurland-2 at Brielle, The Netherlands (an interim report). Mededelingen van de Werkgroep voor Tertiaire en Kwartaire Geologie 25, 49–60.

Meijer, T., 2003. The late Middle Pleistocene non-marine molluscan fauna of borehole Noorderhoeve-19El17 (province of Noord-Holland, The Netherlands). Cainozoic Res. 2, 129–134.

Miller, G.H., Hare, P.E., 1975. Use of amino acid reactions in some Arctic marine fossils as stratigraphic and geochronological indicators. Carnegie Institute of Washington Yearbook 74, 612–617.

Miller, G.H., Mangerud, J., 1985. Aminostratigraphy of European marine interglacial deposits. Quat. Sci. Rev. 4, 215–278. https://doi.org/10.1016/0277-3791(85)90002-2.

Miller, G.H., Beaumont, P.B., Deacon, H.J., Brooks, A.S., Hare, P.E., Jull, A.J.T., 1999. Earliest modern humans in southern Africa dated by isoleucine epimerization in ostrich eggshell. Quat. Sci. Rev. 18, 1537–1548. https://doi.org/10.1016/S0277-3791(99)00044-X.

Nádor, A., Lantos, M., Tóth-Makk, Á., Thamó-Bozsó, E., 2003. Milankovitch-scale multi-proxy records from fluvial sediments of the last 2.6 Ma, Pannonian Basin, Hungary. Quat. Sci. Rev. 22, 2157–2175. https://doi.org/10.1016/S0277-3791(03)00134-3.

Ortiz, J.E., Torres, T., Delgado, A., Julià, R., Lucini, M., Llamas, F.J., Reyes, E., Soler, V., Valle, M., 2004a. The palaeoenvironmental and palaeohydrological evolution of Padul Peat Bog (Granada, Spain) over one million years, from elemental, isotopic and molecular organic geochemical proxies. Organic Geochemistry, Advances in Organic Geochemistry 2003. Organic Geochemistry 35, 1243–1260. https://doi.org/10.1016/j.orggeochem.2004.05.013.

Ortiz, J.E., Torres, T., Julià, R., Delgado, A., Juan Llamas, F., Soler, V., Delgado, J., 2004b. Numerical dating algorithms of amino acid racemization ratios from continental ostracodes. Application to the Guadix-Baza Basin (southern Spain). Quat. Sci. Rev. 23, 717–730. https://doi.org/10.1016/j.quascirev.2003.06.001.

Ortiz, J.E., Torres, T., Delgado, A., Reyes, E., Llamas, J.F., Soler, V., Raya, J., 2006. Pleistocene paleoenvironmental evolution at continental middle latitude inferred from carbon and oxygen stable isotope analysis of ostracodes from the Guadix-Baza Basin (Granada, SE Spain). Palaeogeogr. Palaeoclimatol. Palaeoecol. 240, 536–561. https://doi.org/10.1016/j.palaeo.2006.03.008.

Pajek, L., Tekavec, J., Drešček, U., Lisec, A., Košir, M., 2019. Bioclimatic potential of European locations: GIS supported study of proposed passive building design strategies. In: IOP Conf. Ser.: Environ. Earth Sci., vol. 296, 012008. https://doi.org/10.1088/1755-1315/296/1/012008.

Penck, A., Brückner, E., 1909. Die Alpen im Eiszeitalter, vol. 3. Tauchnitz.

Penkman, K.E.H., Preece, R.C., Keen, D.H., Maddy, D., Schreve, D.C., Collins, M.J., 2007. Testing the aminostratigraphy of fluvial archives: the evidence from intra-crystalline proteins within freshwater shells. Quat. Sci. Rev. 26, 2958–2969.

Penkman, K.E.H., Kaufman, D.S., Maddy, D., Collins, M.J., 2008. Closed-system behaviour of the intra-crystalline fraction of amino acids in mollusc shells. Quat. Geochronol. 3, 2–25. https://doi.org/10.1016/j.quageo.2007.07.001.

Penkman, K.E.H., Preece, R.C., Bridgland, D.R., Keen, D.H., Meijer, T., Parfitt, S.A., White, T.S., Collins, M.J., 2011. A chronological framework for the British Quaternary based on *Bithynia* opercula. Nature 476, 446–449. https://doi.org/10.1038/nature10305.

Penkman, K.E.H., Preece, R.C., Bridgland, D.R., Keen, D.H., Meijer, T., Parfitt, S.A., White, T.S., Collins, M.J., 2013. An aminostratigraphy for the British Quaternary based on *Bithynia* opercula. Quat. Sci. Rev. 61, 111–134. https://doi.org/10.1016/j.quascirev.2012.10.046.

Penkman, K., Thew, N., Presslee, S., Taylor, S., Nelson, E., Kalin, D., Buchi, M., Deplazes, G., 2024. An aminostratigraphy for the Quaternary of the Swiss plateau [preprint]. Anal. Chem. https://doi.org/10.31223/X57700.

Pouloupatis, P.D., Florides, G., Tassou, S., 2011. Measurements of ground temperatures in Cyprus for ground thermal applications. Renew. Energy 36, 804–814. https://doi.org/10.1016/j.renene.2010.07.029.

Powell, J., Collins, M.J., Cussens, J., MacLeod, N., Penkman, K.E.H., 2013. Results from an amino acid racemization inter-laboratory proficiency study; design and performance evaluation. Quat. Geochronol. Amino Acid Racemization 16, 183–197. https://doi.org/10.1016/j.quageo.2012.11.001.

Preece, R.C., Penkman, K.E.H., 2005. New faunal analyses and amino acid dating of the lower palaeolithic site at east farm, Barnham, Suffolk. Proceedings of the Geologists' Association. 116, 363–377. https://doi.org/10.1016/S0016-7878(05)80053-7.

Preece, R.C., Meijer, T., Penkman, K.E.H., Demarchi, B., Mayhew, D.F., Parfitt, S.A., 2020. The palaeontology and dating of the 'Weybourne Crag', an important marker horizon in the Early Pleistocene of the southern North Sea basin. Quat. Sci. Rev. 236, 106177. https://doi.org/10.1016/j.quascirev.2020.106177.

Püspöki, Z., Demeter, G., Tóth-Makk, Á., Kozák, M., Dávid, Á., Virág, M., Kovács-Pálffy, P., Kónya, P., Gyuricza, Gy, Kiss, J., McIntosh, R.W., Forgács, Z., Buday, T., Kovács, Z., Gombos, T., Kummer, I., 2013. Tectonically controlled Quaternary intracontinental fluvial sequence development in the Nyírség-Pannonian Basin, Hungary. Sediment. Geol. 283, 34–56. https://doi.org/10.1016/j.sedgeo.2012.11.003.

Püspöki, Z., Kovács, I.J., Fancsik, T., Nádor, A., Thamó-Bozsó, E., Tóth-Makk, Á., Udvardi, B., Kónya, P., Füri, J., Bendő, Z., Zilahi-Sebess, L., Stercel, F., Gulyás, Á., Mcintosh, R.W., 2016. Magnetic susceptibility as a possible correlation tool in Quaternary alluvial stratigraphy. Boreas 45, 861–875. https://doi.org/10.1111/bor.12196.

Püspöki, Z., Fogarassy-Pummer, T., Thamó-Bozsó, E., Berényi, B., Cserkész-Nagy, Á., Szappanos, B., Márton, E., Lantos, Z., Nádor, A., Fancsik, T., Stercel, F., Tóth-Makk, Á., Mcintosh, R.W., Szőcs, T., Faragó, E., 2020. High-resolution stratigraphy of a Quaternary fluvial deposit based on magnetic susceptibility variations (Jászság Basin, Hungary). Boreas 49, 181–199. https://doi.org/10.1111/bor.12412.

Püspöki, Z., Gibbard, P.L., Nádor, A., Thamó-Bozsó, E., Sümegi, P., Fogarassy-Pummer, T., Mcintosh, R.W., Lantos, M., Tóth-Makk, Á., Stercel, F., Krassay, Z., Kovács, P., Szőcs, T., Fancsik, T., 2021a. Fluvial magnetic susceptibility as a proxy for long-term variations of mountain permafrost development in the Alp-Carpathian region. Boreas 50, 806–825. https://doi.org/10.1111/bor.12520.

Püspöki, Z., Fogarassy-Pummer, T., Thamó-Bozsó, E., Falus, G., Cserkész-Nagy, Á., Szappanos, B., Márton, E., Lantos, Z., Szabó, S., Stercel, F., Tóth-Makk, Á., Mcintosh, R.W., Szőcs, T., Pálóczy, P., Fancsik, T., 2021b. High-resolution stratigraphy of Quaternary fluvial deposits in the Makó Trough and the Danube-Tisza Interfluve, Hungary, based on magnetic susceptibility data. Boreas 50, 205–223. https://doi.org/10.1111/bor.12471.

Püspöki, Z., Gibbard, P.L., Kiss, L.F., McIntosh, R.W., Thamó-Bozsó, E., Krassay, Z., Szappanos, B., Maigut, V., Kovács, P., Karácsony, D., Stercel, F., Visnovitz, F., Demény, K., Bereczki, L., Szőcs, T., Rotár-Szalkai, Á., Fancsik, T., 2023. Obliquity-driven mountain permafrost-related fluvial magnetic susceptibility cycles in the Quaternary mid-latitude long-term (2.5 Ma) fluvial Békés Basin in the Pannonian Basin. Boreas 52, 402–426. https://doi.org/10.1111/bor.12618.

Reille, M., Beaulieu, J.-L.D., Svobodova, H., Andrieu-Ponel, V., Goeury, C., 2000. Pollen analytical biostratigraphy of the last five climatic cycles from a long continental sequence from the Velay region (Massif Central, France). J. Quat. Sci. 15, 665–685. https://doi.org/10.1002/1099-1417(200010)15:7<665::AID-JQS560>3.0.CO;2-G.

Rónai, A., 1985. The Quaternary of the Great Hungarian Plain. Institutum Geologicum Hungaricum.

Royden, L.H., 1988. Late Cenozoic Tectonics of the Pannonian Basin System, vol. 45. AAPG Memoir, pp. 27–48.

Sato, N., Quitain, A.T., Kang, K., Daimon, H., Fujie, K., 2004. Reaction kinetics of amino acid decomposition in high-temperature and high-pressure water. Ind. Eng. Chem. Res. 43, 3217–3222. https://doi.org/10.1021/ie020733n.

Schaefer, I., 1953. Die donaueiszeitlichen Ablagerungen an Lech und Wertach. Geol. Bavarica 19, 13–64.

Singer, B.S., 2014. A Quaternary geomagnetic instability time scale. Quat. Geochron. 21, 29–52.

Tesakov, A.S., Frolov, P.D., Titov, V.V., Dickinson, M., Meijer, T., Parfitt, S.A., Preece, R.C., Penkman, K.E.H., 2020. Aminostratigraphical test of the East European Mammal Zonation for the late Neogene and Quaternary. Quat. Sci. Rev. 245, 106434. https://doi.org/10.1016/j.quascirev.2020.106434.

Thamó-Bozsó, E., Kercsmár, Zs, Nádor, A., 2002. Tectonic control on changes in sediment supply: Quaternary alluvial systems, Körös sub-basin, SE Hungary. In: Jones, S.J., Frostic, L.E. (Eds.), Sediment Flux to Basins: Causes, Controls and Consequences, vol. 191. Geological Society, London, Special Publication, pp. 37–53.

Thamó-Bozsó, E., Kovács, L, Ó., 2007. Evolution of Quaternary to modern fluvial network in the Mid-Hungarian Plain, indicated by heavy mineral distributions and statistical analysis of heavy mineral data. Develpoments in Sedimentaology 58, 491–514.

Tinti, F., Kasmaee, S., Elkarmoty, M., Bonduà, S., Bortolotti, V., 2018. Suitability evaluation of specific shallow geothermal technologies using a GIS-based multi criteria decision analysis implementing the analytic hierarchic process. Energies 11, 457. https://doi.org/10.3390/en11020457.

Tomiak, P.J., Penkman, K.E.H., Hendy, E.J., Demarchi, B., Murrells, S., Davis, S.A., McCullagh, P., Collins, M.J., 2013. Testing the limitations of artificial protein degradation kinetics using known-age massive *Porites* coral skeletons. Quaternary Geochronology, Amino Acid Racemization 16, 87–109. https://doi.org/10.1016/j.quageo.2012.07.001.

Tzedakis, P.C., 1994. Vegetation change through glacial—interglacial cycles: a long pollen sequence perspective. Philosophical Transactions of the Royal Society B 345 (1314), 403–432. https://doi.org/10.1098/rstb.1994.0118.

Tzedakis, P.C., 1999. The last climatic cycle at Kopais, central Greece. J. Geol. Soc. 156, 425–434. https://doi.org/10.1144/gsjgs.156.2.0425.

Tzedakis, P.C., Lawson, I.T., Frogley, M.R., Hewitt, G.M., Preece, R.C., 2002. Buffered tree population changes in a Quaternary refugium: evolutionary implications. Science 297, 2044–2047.

Wehmiller, J.F., 1982. A review of amino acid racemization studies in Quaternary mollusks: stratigraphic and chronologic applications in coastal and interglacial sites, Pacific and Atlantic coasts, United States, United Kingdom, Baffin Island, and tropical islands. Quat. Sci. Rev. 1, 83–120. https://doi.org/10.1016/0277-3791(82)90001-4.

Wehmiller, J.F., Hall, F.R., 1997. 22. Data Report: amino acid racemization geochronological studies of selected leg 155 samples. In: Proceedings of the Ocean Drilling Program. Scientific Results.

Wehmiller, J., Miller, G.H., 2000. Aminostratigraphic dating methods in Quaternary geology. In: Noller, J.S., Sowers, J.M., Lettis, W.R. (Eds.), Quaternary Geochronology: Methods and Applications. American Geophysical Union, Washington D.C, pp. 187–222.

Wehmiller, J.F., Stecher, H.A., 2000. The thermal environment of fossils: effective ground temperatures at aminostratigraphic sites on the U.S. coastal plain. In: Perspectives in Amino Acid and Protein Geochemistry. Oxford University Press, United Kingdom, pp. 219–252.

Wehmiller, J.F., Thieler, E.R., Miller, D., Pellerito, V., Bakeman Keeney, V., Riggs, S.R., Culver, S., Mallinson, D., Farrell, K.M., York, L.L., Pierson, J., Parham, P.R., 2010. Aminostratigraphy of surface and subsurface Quaternary sediments, North Carolina coastal plain, USA. Quat. Geochronol. 5, 459–492. https://doi.org/10.1016/j.quageo.2009.10.005.

Wenau, S., Alves, T.M., 2020. Salt-induced crestal faults control the formation of Quaternary tunnel valleys in the southern North Sea. Boreas 49, 799–812. https://doi.org/10.1111/bor.12461.

West, G., Kaufman, D.S., Muschitiello, F., Forwick, M., Matthiessen, J., Wollenburg, J., O'Regan, M., 2019. Amino acid racemization in Quaternary foraminifera from the yermak plateau, arctic ocean. Geochronology 1, 53–67. https://doi.org/10.5194/gchron-1-53-2019.

Wheeler, L.J., Penkman, K.E.H., Sejrup, H.P., 2021. Assessing the intra-crystalline approach to amino acid geochronology of *Neogloboquadrina pachyderma* (sinistral). Quat. Geochronol. 61, 101131. https://doi.org/10.1016/j.quageo.2020.101131.